Plasticity in AAA+ proteases reveals ATP-dependent substrate specificity principles

Samar A. Mahmoud[1,2], Berent Aldikacti[1,2], Peter Chien[1,2*]

Affiliations:

[1]Department of Biochemistry and Molecular Biology, [2]Molecular and Cellular Biology Program, University of Massachusetts Amherst, Amherst, MA 01003, USA.

Corresponding Author:

Peter Chien
240 Thatcher Rd, Amherst, MA 01003
pchien@umass.edu
(413) 545-2310

Graphical Abstract

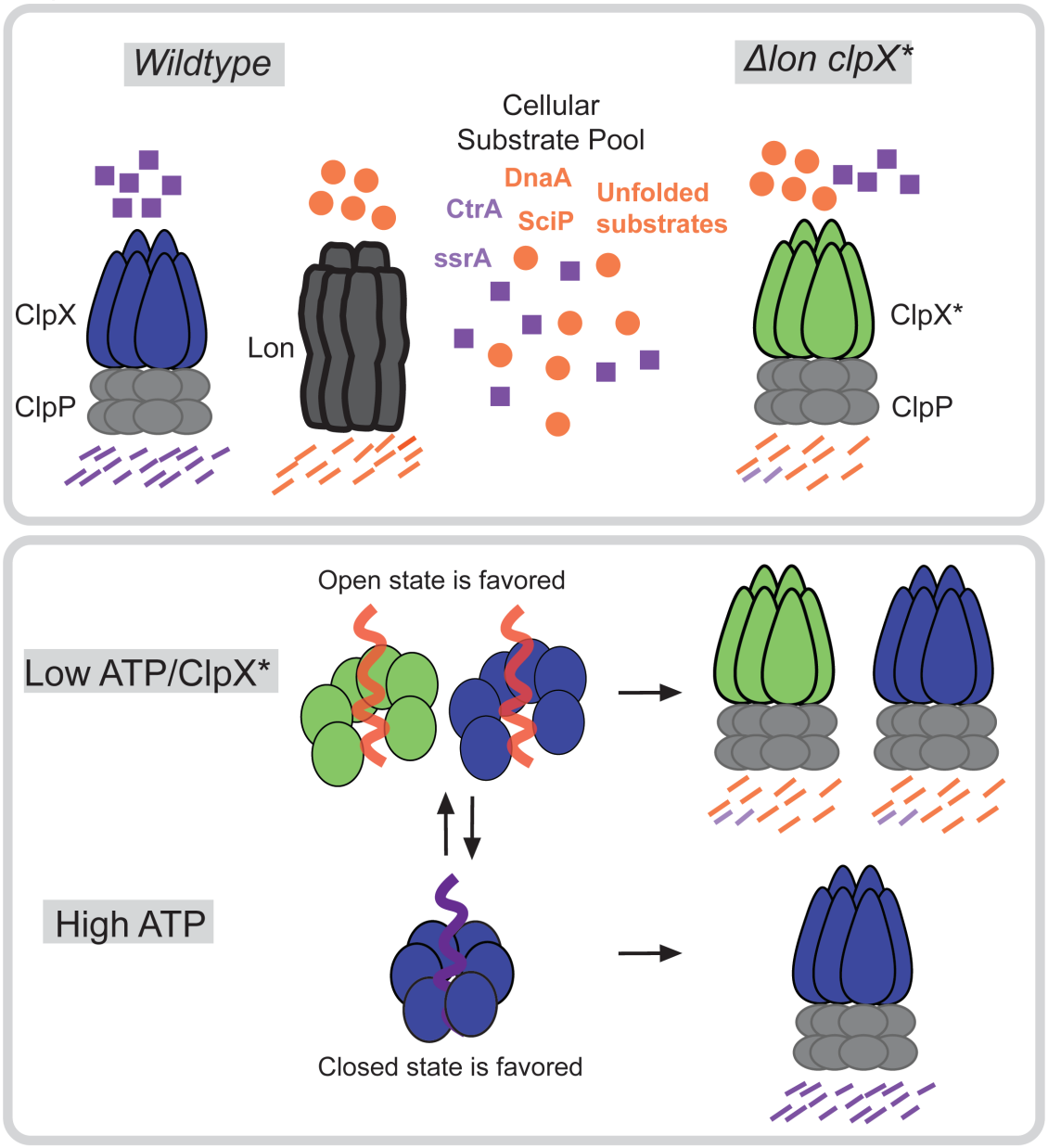

In a wildtype cell, AAA+ proteases Lon and ClpXP promote normal growth by degrading distinct substrates. ClpX*P can compensate for the absence of the Lon protease by tuning ClpXP substrate specificity to better degrade Lon-privileged substrates (such as DnaA, SciP, and misfolded proteins) but this comes at the cost of native ClpXP substrates (such as ssrA-tagged proteins and CtrA). We propose that ClpX alternates between a closed and open conformation and promoting one state over the other leads to alterations in substrate specificity. In the presence of ClpX* or in ATP-limited conditions, the open state is favored, allowing capture and recognition of substrates such as casein. The balance shifts to the closed state under high ATP conditions, allowing degradation of substrates such as GFP-ssrA, which preferentially bind the closed state.

Summary

In bacteria, AAA+ proteases such as Lon and ClpXP specifically degrade substrates to promote growth and stress responses. Here, we find that an ATP-binding mutant of ClpX suppresses physiological defects of a Lon-deficient strain by shifting ClpXP protease specificity toward normally Lon-restricted substrates and away from normal ClpXP targets. Reconstitution with purified proteins assigns these effects to changes in direct recognition and processing of substrates. We show that wildtype ClpXP specificity can be similarly altered when ATP hydrolysis is reduced, which unexpectedly accelerates degradation of some substrates. This activation corresponds with changes in ClpX conformation, leading to a model where ClpX cycles between 'capture' and 'processive' states depending on ATP loading. Limiting ATP binding alters dynamics between states affording better recognition of unorthodox substrates, but worse degradation of proteins specifically bound by the processive state. Thus, AAA+ protease specificities can be directly tuned by differences in ATP hydrolysis rates.

Highlights

- A mutation in the Walker B region of ClpX induces recognition of new substrates.
- Proteases are optimized for specific functions but barrier to recognize new substrates is easily overcome.
- Expanding substrate recognition by a protease comes at the cost of reducing native substrate degradation.
- Decreasing ATP enhances ClpXP mediated degradation of certain classes of substrates.
- ClpX adopts distinct conformational states to favor better recognition of some substrates over others.

Introduction

Energy-dependent protein degradation regulates normal growth and stress responses in all cells. In bacteria, regulated proteolysis is carried out by several energy-dependent AAA+ (ATPases associated with cellular activities) proteases which include Lon, ClpXP,

84 ClpAP, HslUV, FtsH (Gur et al., 2011; Mahmoud and Chien, 2018). These proteases
85 share a similar general architecture containing an unfoldase domain and a non-specific
86 peptidase (Sauer and Baker, 2011). The two domains can be encoded on a single
87 polypeptide, such as in the case of Lon and FtsH, or they can be encoded by separate
88 proteins, an ATPase, such as ClpX, and a peptidase, such as ClpP (Baker and Sauer,
89 2012; Langklotz et al., 2012; Lee and Suzuki, 2008). Using the power of ATP hydrolysis,
90 the unfoldase recognizes, unfolds, and translocates substrates into the sequestered
91 peptidase chamber to be degraded. Because they are critical for maintaining
92 proteostasis, loss of these proteases results in defects in growth, cell-cycle progression,
93 stress responses, and pathogenesis (Breidenstein et al., 2012; Howard-Flanders et al.,
94 1964; Jenal and Fuchs, 1998; Rogers et al., 2016).
95
96 Despite the similarities in both architecture and mechanism, these proteases generally
97 have distinct niches of substrate preference. For example, in *Caulobacter crescentus*,
98 Lon is the principal protease for degradation of the replication initiator DnaA (Jonas et
99 al., 2013), the methyltransferase CcrM (Wright et al., 1996), and the transcriptional
100 regulator SciP (Gora et al., 2013). By contrast, the ClpXP protease degrades cell-cycle
101 factors like CtrA and TacA during cell-cycle progression through an adaptor hierarchy
102 (Joshi et al., 2015). Lon is also responsible for misfolded protein degradation
103 (Goldberg, 1972; Gur and Sauer, 2008; Jonas et al., 2013). However, while a handful of
104 target substrates for these AAA+ have been identified, it remains unclear how proteases
105 are able to discriminate among protein targets and recognize distinct substrates for
106 irreversible degradation.
107
108 In this work, we find that a variant of ClpX (*clpX**) can compensate for the absence of
109 the Lon protease. Expression of *clpX** suppresses defects in motility, growth,
110 filamentation, and sensitivity to stress normally seen in a Δ*lon* strain. In addition to this
111 phenotypic rescue, degradation of normal Lon substrates is restored *in vivo* and *in vitro*
112 by ClpX*P. This increased ability to degrade noncanonical substrates comes at the cost
113 of reduced degradation of ClpXP-specific substrates, resulting in fitness defects in
114 otherwise wildtype strains expressing the *clpX** allele. Further mechanistic

115 characterization shows that ClpX* has reduced catalytic efficiency for ATP hydrolysis,
116 suggesting a connection between ATP utilization and substrate specificity. Consistent
117 with this, limiting ATP for wildtype ClpXP shifts substrate preferences to that of ClpX*P.
118 Limited proteolysis shows that the ClpX unfoldase adopts distinct conformations under
119 these ATP limiting or saturating conditions. Taken together, our work demonstrates that
120 ATP-dependent dynamics between conformational states are important for substrate
121 recognition by AAA+ unfoldases.
122
123 **Results**
124 **A suppressor screen identifies a *clpX* mutant which rescues *Δlon***
125 We reasoned that a suppressor screen would allow us to identify novel Lon-related
126 interactions and used a transposon library to identify mutations that restore motility to a
127 *Δlon* strain. We isolated a high motility mutant with a transposon insertion in
128 CCNA_00264; however transduction experiments revealed that this transposon alone
129 was not able to rescue motility (Figure S1A). Sequencing the genome of the suppressor
130 strain showed a point mutation in *clpX*, which resulted in a single amino acid change
131 from glycine 178 to alanine (*clpX**). This glycine is highly conserved among ClpX
132 homologs and immediately adjacent to the Walker B motif (Figure S1C). By generating
133 the *clpX** allele in a *Δlon* background, we found that *clpX** on its own partially restores
134 motility (Figure 1A).
135
136 We were intrigued that a single mutation in *clpX* could restore motility to cells lacking
137 Lon and chose to further characterize this strain. Cells lacking Lon show growth defects
138 that exhibit as an extended lag phase and reduced cell mass accumulation in stationary
139 phase (Figure 1A). The *clpX** allele rescues the mass accumulation defect, but not the
140 extended lag (Figure 1A). *Δlon* strains also have significant morphological deficiencies
141 including elongated cell length and longer stalks, external polar organelles characteristic
142 of *Caulobacter*. We found that the *clpX** mutant restored the cell length of Δ*lon* strains to
143 near wildtype levels (Figure 1B, 1C). However, stalks remained elongated in the *Δlon*
144 *clpX** strain (Figure 1B, 1C).
145

146 We next wondered if, in addition to suppression of *Δlon* morphological and growth
147 defects, sensitivity to certain stressors would be suppressed by this *clpX** allele. One of
148 the originally described phenotypes for *E. coli lon* mutants is DNA damage sensitivity
149 (Mizusawa and Gottesman, 1983; Witkin, 1946) and *Caulobacter ΔIon* strains are also
150 highly sensitive to various DNA damaging agents (Zeinert et al., 2018), including
151 mitomycin C (Figure 1C). We found that Δ*lon clpX** was 100-fold more resistant to MMC
152 than *Δlon* alone (Figure 1C).
153
154 As mentioned previously, Lon is the major protease responsible for the degradation of
155 the replication initiator DnaA and *Δlon* strains accumulate excess chromosome content
156 (Jonas et al., 2013; Wright et al., 1996). Like the morphological abnormalities,
157 overreplication is suppressed in the Δ*lon clpX** strain which shows similar chromosome
158 content as wildtype cells (Figure 1D, S1D). To determine if this rescue extended to a
159 systems-level correction, we compared RNA-seq profiles of wildtype, Δ*lon* and Δ*lon*
160 *clpX** strains. As expected, many genes (435) are differentially expressed upon loss of
161 Lon (Figure 1E), while the Δ*lon clpX** strain shows fewer differences (119) with only 85
162 genes overlapping between these sets. Our interpretation is that expression of *clpX** in
163 a Δ*lon* background largely shifts the phenotypes and transcriptional landscape to more
164 wildtype profiles.

Figure 1

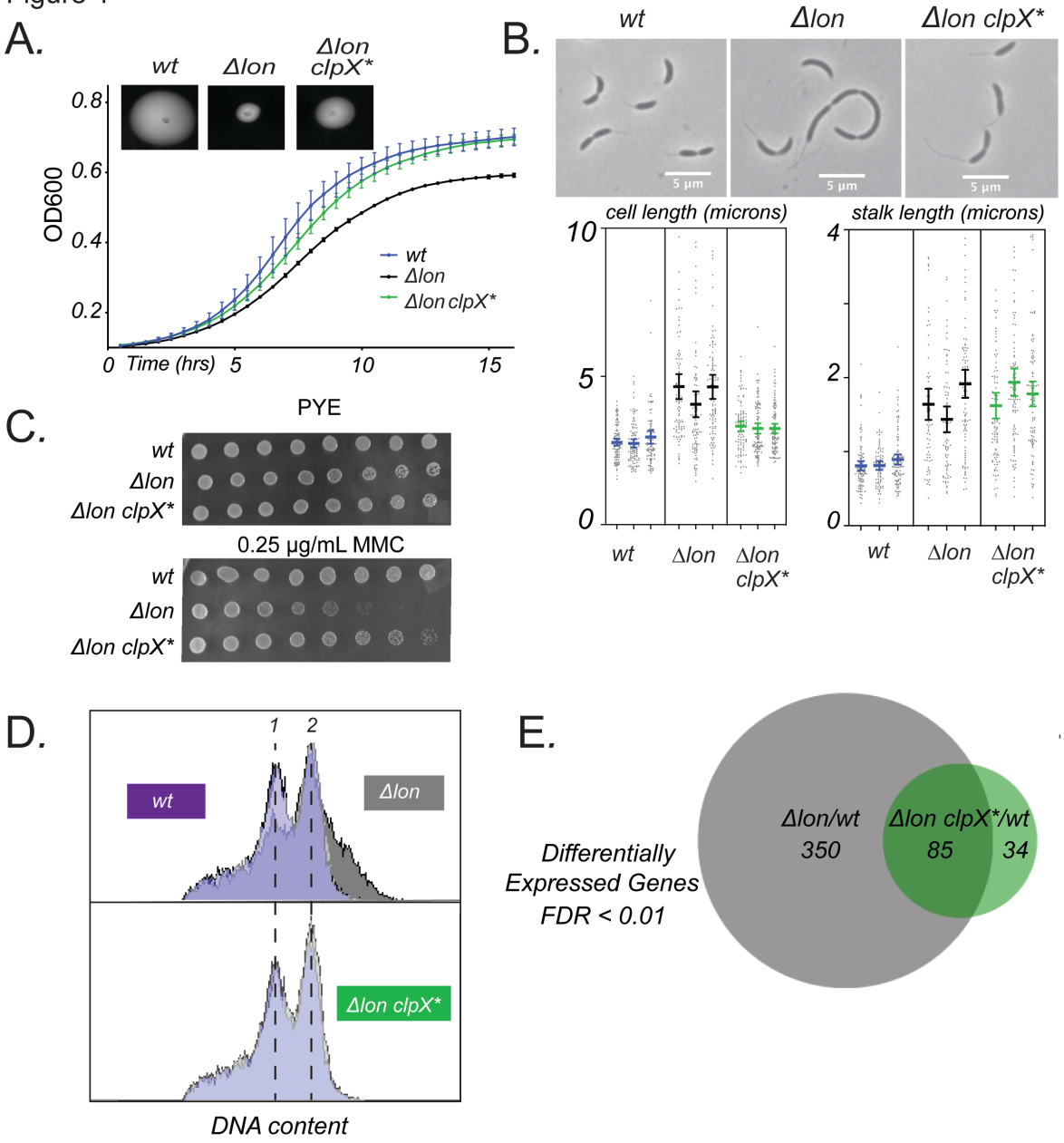

Figure 1: *clpX mutant suppresses *Δlon* phenotypes**

A. Growth curves of *wild type* (*wt*), *Δlon, and Δlon clpX** cells grown in PYE. Biological triplicate experiments are shown. Error bars represent 95% confidence interval. Inset shows motility assays as measured by growth in 0.3% PYE agar.

B. Representative phase-contrast microscopy images of *wt*, *Δlon, and Δlon clpX** cells grown in PYE during exponential phase. Quantification of cell length and stalk length for three biological replicates of n=100 cells.

C. Serial dilution assays comparing colony formation of strains in PYE and PYE supplemented with mitomycin C. Spots are plated 10-fold dilutions of exponentially growing cells from left to right.

176 D. Flow cytometry profiles showing chromosome content of indicated strains after three-
177 hour treatment with rifampicin. Cells were stained with SYTOX Green to measure DNA
178 content. The fluorescent intensities corresponding to one chromosome (1) and two
179 chromosomes (2) are indicated. Experiment was performed two times. Representative
180 data from one of the biological replicates is shown here.
181 E. Venn diagram summarizing the number of differentially expressed genes with an
182 FDR cutoff < 0.01 from RNA seq performed with stationary phase cells. Venn diagram
183 created by BioVenn (Hulsen et al., 2008).
184
185 See also Figure S1.
186
187 **ClpX* restores degradation of Lon substrates *in vivo***
188 Because cells lacking Lon would accumulate normally degraded substrates, we
189 hypothesized that the rescue we observed in the *Δlon clpX** strain was likely due to
190 lower levels of Lon substrates, such as DnaA, CcrM, and SciP (Figure 2A) (Gora et al.,
191 2013; Jonas et al., 2013; Wright et al., 1996). As expected, in unsynchronized cells,
192 DnaA and CcrM levels are higher in the Δ*lon* strain than in wildtype (Figure 2B).
193 Similarly, SciP levels are higher in Δ*lon* swarmer cells in comparison to wildtype (Figure
194 2D). Interestingly, levels of DnaA and SciP are restored to wildtype levels in the Δ*lon*
195 *clpX** strain; however, CcrM remained at higher levels (Figure 2B). The reduced levels
196 of DnaA likely explain the rescue of replication defects and enrichment analysis of the
197 RNA-seq results shows that the SciP-controlled regulon and cell-cycle gene expression
198 are largely restored in the Δ*lon clpX** strain (Figure S2). We reasoned that expression
199 of *clpX** rescues normal growth and critical stress responses in a Δ*lon* strain through
200 restoring wildtype levels of key proteins.
201
202 Next, we explored the mechanism by which a mutation in ClpX is able to restore steady
203 state levels of DnaA and SciP. Because DnaA and SciP are controlled by proteolysis,
204 we suspected that protein turnover may be affected. As expected, DnaA is largely
205 stabilized in Δ*lon* strains (Figure 2C; Jonas, et al. 2013); however, we found that DnaA
206 degradation was restored in the Δ*lon clpX** *strain*, with a half-life similar to that of
207 wildtype (Figure 2D). SciP protein dynamics and cell-cycle phase specific levels were
208 also restored in Δ*lon clpX** cells (Figure 2D). By contrast, CcrM degradation was still

209 solely dependent on Lon, even when *clpX** was present, in both unsynchronized cells
210 (Figure 2C) and during cell-cycle progression (Figure S3A).
211
212 We considered that changes in protein turnover could be either due to a gain-of-function
213 in the *clpX** mutant or by indirect cellular effects associated with a loss-of-function in
214 *clpX*. To test this, we created a merodiploid *Δlon* strain expressing a second copy of
215 *clpX* or *clpX** under control of the native promoter along with a normal chromosomal
216 copy of *clpX*. We reasoned that if the effect was direct, then expression of *clpX** would
217 be sufficient to restore DnaA degradation. If the effect was indirect, then DnaA would
218 remain stable. Consistent with a gain-of-function phenotype for the *clpX** allele, we
219 found that DnaA turnover increased upon expression of *clpX** but not wildtype *clpX*
220 (Figure 2E). Similarly, the phenotypic rescue we observed in the *Δlon clpX** strain was
221 also due to a gain-of-function activity as the merodiploid strain expressing *clpX**
222 suppressed *Δlon* defects, such as growth, motility, and genotoxic stress tolerance
223 (Figure S3B-D). Because ClpXP is a AAA+ protease, we hypothesized that ClpX*P (the
224 protease complex of the variant ClpX* with wildtype ClpP) was now able to recognize
225 and degrade substrates normally degraded by Lon.

Figure 2

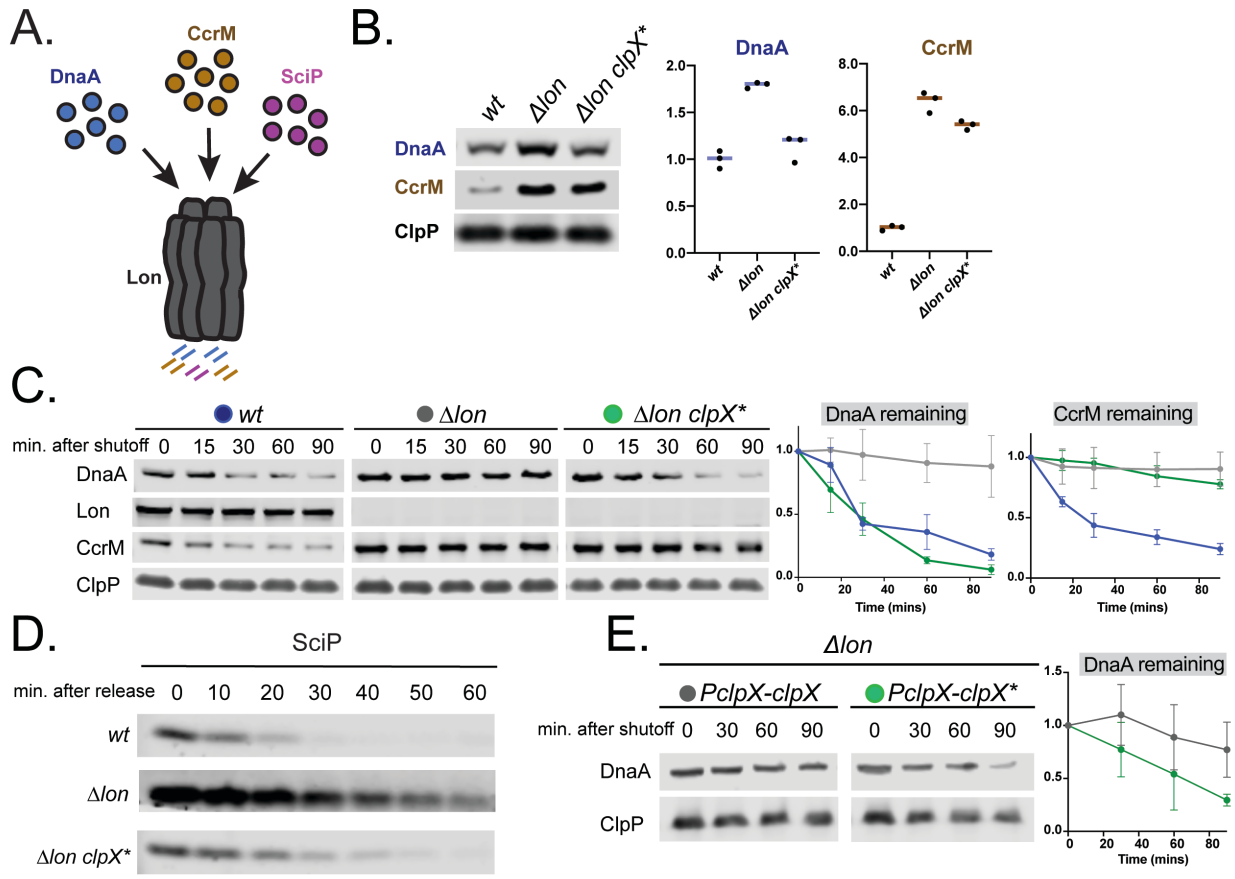

Figure 2: *clpX mutant restores levels of Lon substrates through degradation**

A. Lon degrades DnaA, SciP, and CcrM in *C. crescentus* (Wright *et al.*, 1996; Gora *et al.*, 2013; Jonas *et al.*, 2013).

B. Western blot showing DnaA and CcrM levels in *wt*, *Δlon, and Δlon clpX** cells. Lysates from an equal number of exponential phase cells were probed with anti-DnaA or anti-CcrM antibody. ClpP was used as a loading controls. A representative image and quantifications of triplicate experiments are shown.

C. Antibiotic shutoff assays to monitor DnaA and CcrM stabilities in wt*, Δlon, and Δlon clpX** cells. Chloramphenicol was added to stop synthesis and lysates from samples at the indicated time points were used for western blot analysis. Quantifications of triplicate experiments with substrate shown relative to ClpP control levels are shown to the right. Error bars represent SD.

D. Western blot showing SciP levels in synchronized populations of wt, *Δlon, and Δlon clpX** cells. Swarmer cells were isolated using a density gradient and an equal number of cells were released into fresh PYE medium. Samples were withdrawn at the indicated time points and probed with anti-SciP.

E. DnaA stability is measured in *Δlon* strains expressing an extra copy of wildtype *clpX* or *clpX**. Experiment was performed four times. Representative data from one of the biological replicates is shown here. Quantifications of experiments shown to the right. Error bars represent SD.

247
248 See also Figure S2 and S3.
249

250 **ClpX*P directly degrades Lon substrates *in vitro***

251 As a direct test of our hypothesis, we purified the ClpX* variant and reconstituted
252 degradation *in vitro*. Upon initial characterization of purified ClpX*, we found that it
253 formed an active ATPase, but hydrolyzed ATP three times faster than wildtype (Figure
254 S4A). Consistent with the fact that Lon is the principal protease for DnaA degradation
255 (Jonas et al., 2013; Liu et al., 2016), we found that wildtype ClpXP poorly degraded
256 DnaA *in vitro* (Figure 3A). However, purified ClpX*P could degrade DnaA four-fold
257 faster than ClpXP (Figure 3A). Similarly, SciP was degraded three-fold faster by ClpX*P
258 in comparison to ClpXP (Figure 3A). Finally, as predicted from our *in vivo* results, CcrM
259 was not degraded by either ClpX*P or ClpXP (Figure 3A, Figure S4B), but was well
260 degraded by Lon (Figure S4B). Thus, ClpX* appears to have an expanded substrate
261 profile which includes some Lon substrates, but others, such as CcrM, remain exclusive
262 to Lon.
263

264 Lon recognizes exposed hydrophobic amino acids (Gur and Sauer, 2008) and is best
265 known as a quality control protease that eliminates mis/unfolded proteins (Goff et al.,
266 1984). Given its altered specificity, we considered if ClpX* could now recognize these
267 substrates. Casein is commonly used as an *in vitro* model substrate for mis/unfolded
268 proteins. Lon robustly degrades fluorescently labeled casein, whereas wildtype ClpXP
269 poorly degrades this substrate (Figure 3B). Intriguingly, ClpX*P degrades FITC-casein
270 more than twice as fast as ClpXP (Figure 3B, Figure S4C). Similar to casein, ClpX*P
271 degrades another unfolded Lon substrate, a chemically denatured domain of titin tagged
272 with the hydrophobic sequence β20, better than wildtype ClpXP (Figure S4D).
273

274 Because cells lacking Lon are sensitive to proteotoxic stresses that create misfolded
275 proteins and because ClpX*P is better at degrading mis/unfolded substrates than
276 wildtype ClpXP, we wondered if the Δ*lon clpX** strain would be more resistant to
277 stressors that induce cellular protein misfolding. Indeed, the presence of the *clpX** allele
278 protected Δ*lon* cells from hypersensitivity to the proteotoxic amino acid L-canavanine

279 (Figure 3B). We conclude that ClpX* has an altered substrate preference, that includes
280 DnaA, SciP, and unfolded proteins, whose degradation are normally governed by the
281 Lon protease.

Figure 3

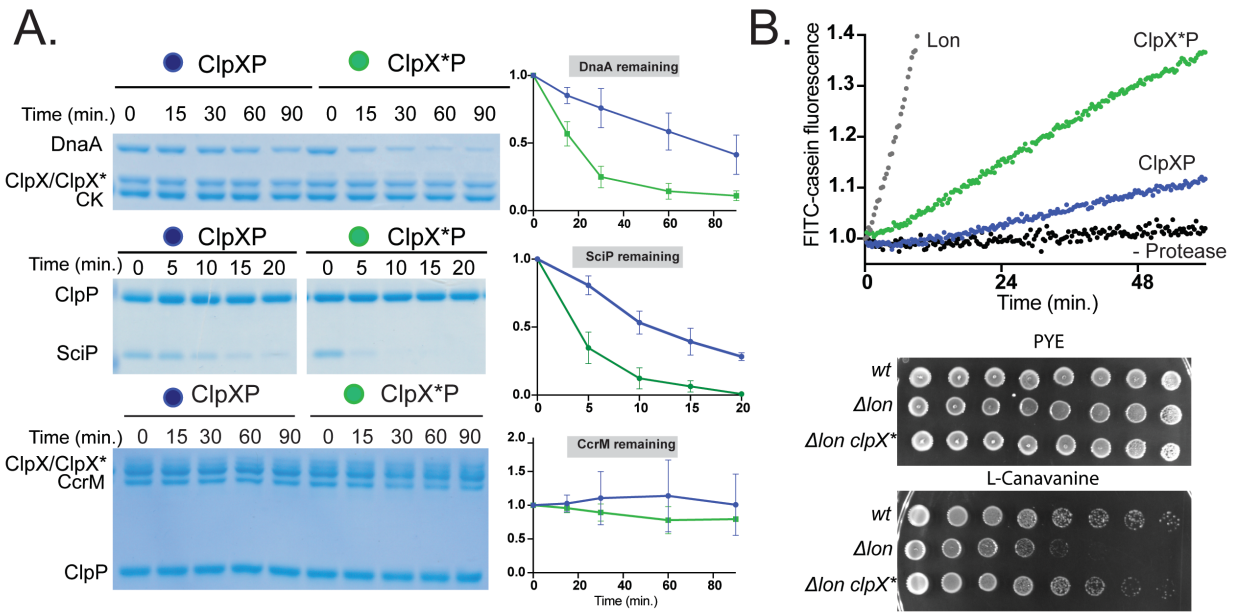

282

283 **Figure 3: ClpX*P degrades some Lon substrates faster than ClpXP in vitro.**
284 A. *In vitro* degradation of DnaA, SciP, or CcrM. Assays were performed with 0.1 μM
285 $ClpX_6$ or $ClpX_6$*, and 0.2 μM $ClpP_{14}$. Substrate concentrations were 1 μM DnaA, 5 μM
286 SciP, 0.5 μM CcrM. Quantification of triplicate experiments shown. Error bars represent
287 SD.
288 B. *In vitro* fluorescence degradation assay of FITC-casein in the presence of ClpXP or
289 ClpX*P or Lon. Degradation assays were performed with 10μg/mL FITC-Casein, 0.1 μM
290 $ClpX_6$ or $ClpX_6$* and 0.2 μM ClpP or 0.1 μM Lon_6. Serial dilution assays comparing
291 colony formation of strains in PYE and PYE supplemented with L-canavanine. Spots are
292 plated 10-fold dilutions of exponentially growing cells from left to right.
293
294 See also Figure S4.
295

296 **ClpX*P is deficient in degradation of native ClpXP substrates**

297 Mutations in ClpX that improve recognition of some substrates can have negative
298 consequences on others (Farrell et al., 2007). GFP-ssrA is a well-characterized ClpXP
299 substrate that is directly bound by the pore loops of ClpX (Fei et al., 2020; Gottesman et
300 al., 1998). We purified GFP fused to the *Caulobacter* ssrA tag (Chien, et al. 2007),
301 determined degradation rates by ClpX*P and ClpXP, and fit these rates to the
302 Michaelis-Menten equation. We found that ClpX*P degrades GFP-ssrA more poorly

303 than wildtype ClpXP, principally lowering the turnover rate (Figure 4A, Figure S5A),
304 suggesting that either ClpX* fails to bind the ssrA tag as readily or is unable to
305 translocate the reporter protein as well as ClpX. This effect was not due to the GFP as
306 an ssrA-tagged unfolded titin domain was also degraded more slowly by ClpX*P (Figure
307 S5B). Given that the β20-tagged version of this same construct was degraded more
308 rapidly, we conclude that the altered specificity of ClpX* must rely on the recognition tag
309 identity, rather than on changes in substrate translocation
310
311 CtrA is a master regulator in *Caulobacter* that inhibits replication initiation and regulates
312 the transcription of many cell-cycle genes (Laub et al., 2002; Wortinger et al., 2000). *In*
313 *vivo*, CtrA is degraded during the G1-S transition by ClpXP through the use of an
314 adaptor hierarchy (Domian et al., 1999; Jenal and Fuchs, 1998; Joshi et al., 2015; Quon
315 et al., 1996); however, *in vitro* CtrA can also be directly recognized by ClpXP as its C-
316 terminus resembles the ssrA tag (Chien et al., 2007). Consistent with a reduced ability
317 to recognize ClpXP substrates, ClpX*P degrades isolated CtrA more poorly than
318 wildtype (Figure 4B) and also shows reduced degradation of a CtrA-derived GFP
319 reporter (Smith et al., 2014) in the presence of the full adaptor hierarchy (Figure S5C).
320 We conclude that ClpX*P overall has a diminished ability to recognize and degrade
321 native substrates normally degraded by ClpXP.
322
323 **Deficiencies of ClpX* revealed when Lon is present**
324 The prior *in vitro* data suggests that rather than just expanding specificity, this mutation
325 has allowed ClpX*P to degrade Lon-dependent substrates better but at the cost of
326 degrading ClpXP-dependent ones. If this is true, while *clpX** is beneficial in a *Δlon*
327 background, we reasoned that it may be detrimental to *lon*$^+$ cells.
328
329 To test this hypothesis, we generated a strain with *clpX** as its sole copy. We first
330 examined ssrA tag turnover in this strain by using an ssrA derivative that relies on the
331 SspB adaptor for degradation (eGFP-ssrA(DAS)) (Chowdhury et al., 2010) so that
332 degradation would be sufficiently slowed to be visualized by western blotting.
333 Consistent with our *in vitro* experiments, we observed stabilization and dramatically

334 higher levels of eGFP-ssrA (DAS) in the *clpX** strain in comparison to wildtype (Figure
335 4C). We observed reduced CtrA degradation in the *clpX** strain, consistent with our *in*
336 *vitro* observations (Figure 4C). Finally, DnaA degradation is accelerated in the *clpX**
337 strains compared to wildtype – consistent with our findings that both Lon and ClpX*P
338 are able to degrade DnaA (Figures 4C).
339
340 We assayed the overall physiological consequence of ClpX* using competitive fitness in
341 mixed cultures. We grew cultures of wildtype *clpX* or the *clpX** strain together with
342 wildtype strains constitutively expressing the Venus fluorescent protein (Persat et al.,
343 2014). We found that while nonfluorescent wildtype cells could slightly outcompete the
344 constitutive Venus expressing cells, the *clpX** strain showed a substantial competitive
345 disadvantage (Figure 4D). We also tested for stress tolerances and found that *clpX**
346 strains fail to survive genotoxic stress as robustly as wildtype (Figure 4E). Our
347 conclusion is that reduced fitness of the wildtype *clpX** strain is likely due to reduced
348 degradation of normal ClpXP substrates (such as CtrA) and prolific degradation of
349 normal Lon substrates (such as DnaA) that together reduce overall fitness. Collectively,
350 this supports our understanding that AAA+ proteases have been optimized for specific
351 priorities in a cell – expansion of their substrate profile, as seen with *clpX*,* can
352 compensate for loss of other proteases, but at the cost of their ability to recognize their
353 normal substrates.

Figure 4

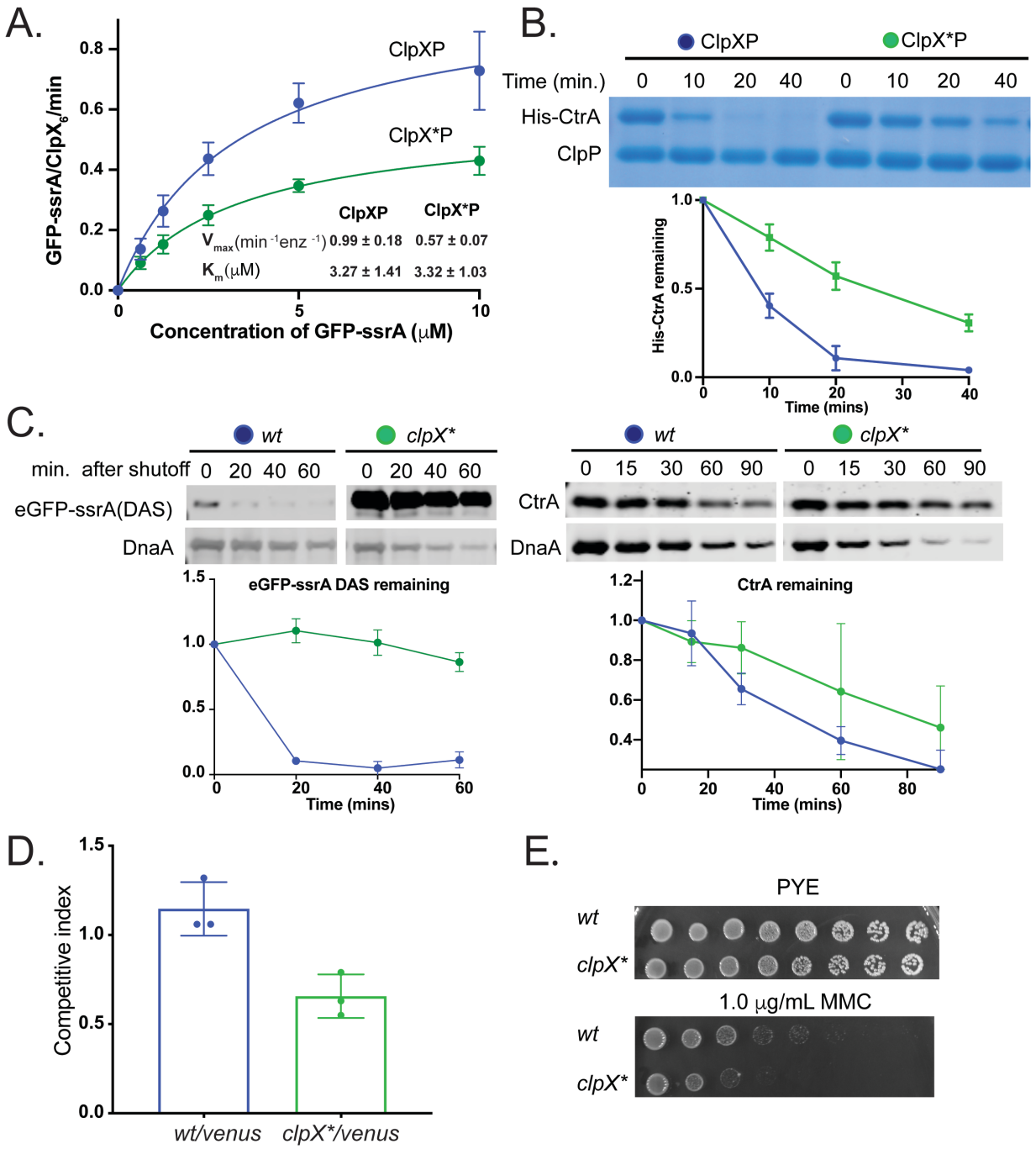

354

355 **Figure 4: ClpX* mutant is deficient in degradation of native ClpXP substrates**
356 A. Michaelis-Menten plot showing the rate of degradation as a function of GFP-ssrA
357 concentration by ClpXP and ClpX*P. Inset displays kinetic parameters. Assays were
358 performed with 0.1 μM ClpX or ClpX* hexamer, 0.2 μM ClpP, ATP regeneration system,
359 and the indicated concentrations of GFP-ssrA. Data was fitted to Michaelis-Menten
360 equation. Triplicate experiments are shown.

361 B. *In vitro* degradation assay of His-CtrA in the presence of ClpXP or ClpX*P.
362 Degradation assays were performed with 3 μM His-CtrA, 0.1 μM ClpX or ClpX*
363 hexamer, 0.2 μM ClpP, and ATP regeneration system. Quantification of duplicate
364 experiments is shown below. Error bars represent SD.
365 C. *In vivo* degradation assay showing eGFP-ssrA (DAS), DnaA, and CtrA stability in *wt*
366 and *clpX** cells. The plasmid encoded M2FLAG-eGFP-ssrA (DAS) construct was
367 induced with the addition of 0.2% xylose. Chloramphenicol was used to inhibit protein
368 synthesis. Samples were withdrawn at the indicated time points and quenched in SDS
369 lysis buffer. Lysate from an equal number of cells was used for western blot analysis
370 and probed with anti-M2, or anti-CtrA, and anti-DnaA antibody. Quantification of
371 triplicate experiments is shown below. Error bars represent SD.
372 D. Competition assay with wildtype cells harboring xylX::Plac-venus (constitutive venus
373 expression) and nonfluorescent wt or *clpX** strains. exponential phase cells were mixed
374 1:1, diluted, and allowed to outgrow for 12 doublings. . Quantification of triplicate
375 experiments is shown below. Error bars represent SD.
376 E. Serial dilution assays comparing colony formation of *wt* and *clpX** cells in PYE and
377 PYE supplemented with MMC. Spots are plated 10-fold dilutions of exponentially
378 growing cells from left to right.
379
380 See also Figure S5.
381

382 **Limiting ATP alters wildtype ClpXP substrate specificity**

383 To understand how this mutation in ClpX leads to enhanced degradation of certain
384 substrates, we further characterized the ATPase activity of ClpX*. While ClpX*
385 hydrolyzes ATP three-fold faster than wildtype ClpX at saturating ATP concentrations
386 (Figure S4A), Michaelis-Menten experiments showed that the K_M increases by 5-6 fold
387 and the catalytic efficiency for ATP hydrolysis decreases by approximately 2 fold,
388 suggesting that ClpX* has a different relationship with ATP compared to wildtype ClpX
389 (Figure 5A). As seen previously, degradation of GFP-ssrA was precipitously lost below
390 a minimum threshold of ATP (Martin et al., 2008), with the ClpX*P threshold being
391 higher than that of wildtype, consistent with the higher K_M for ATP described above
392 (Figure S6A). For ClpX*P, casein degradation reduced monotonically as ATP
393 concentration was lowered (Figure 5B). In striking contrast, we found that for wildtype
394 ClpXP, casein degradation was increased at intermediate nucleotide concentrations
395 compared to saturating ATP (Figure 5B). Kinetic analysis shows that at these lower
396 ATP concentrations ClpXP degrades casein with a lower K_M and a similar V_{max}
397 compared to saturating ATP conditions (Figure 5C). Since $K_M = K_D + k_{cat}/k_{on}$, the lower

398 K_M rate suggests that, at a minimum, casein must bind better to ClpX at these
399 concentrations.
400
401 These results suggest that ClpX specificity depends on ATP concentration in an
402 unexpected fashion, with lower levels of ATP facilitating ClpX recognition of some
403 substrates. We reasoned that this could explain the altered specificity of the ClpX*
404 mutant, as its increased K_M for ATP may allow ClpX* to resemble this low ATP state
405 even under saturating ATP conditions (Figure 5A). Remarkably, this enhanced
406 degradation at low ATP extended to other ClpX* substrates, such as DnaA and SciP
407 (Figure 5D and S6B). We conclude that ClpX preference depends on ATP state, with its
408 specificity expanded when not fully loaded with ATP.
409
410 This *in vitro* data suggests that ClpXP may play a role in better degrading some
411 substrates such as DnaA *in vivo* under ATP limiting conditions. To test this, we
412 monitored degradation of DnaA during starvation using a Δ*lon* Δ*clpA* strain which should
413 eliminate any non-ClpX dependent degradation (Liu et al., 2016). Glucose starvation
414 has been shown to accelerate DnaA degradation (Gorbatyuk and Marczynski, 2005)
415 which we found true for wildtype cells as well (Figure 5E). Importantly, starving Δ*lon*
416 Δ*clpA* also markedly increased DnaA degradation (Figure 5E) concurrent with a
417 reduction in ATP levels (Figure S6C).
418
419 We considered conformational changes in ClpX that might explain the altered specificity
420 at low ATP. Using limited proteolysis to probe conformational differences we found that
421 ClpX at low ATP was more protease accessible than at high ATP (Figure 5F).
422 Consistent with the shared altered specificity, protease accessibility of ClpX* at high
423 ATP was more similar to wildtype ClpX at low ATP than high (Figure 5F). This suggests
424 that a more open structure of ClpX is present at low ATP and with ClpX* that allows it to
425 recognize some substrates more readily. We hypothesize that this low ATP-induced
426 conformational difference may reflect the observed changes in AAA+ structures seen in
427 recent cryo-EM studies and discuss their ramifications below.

Figure 5

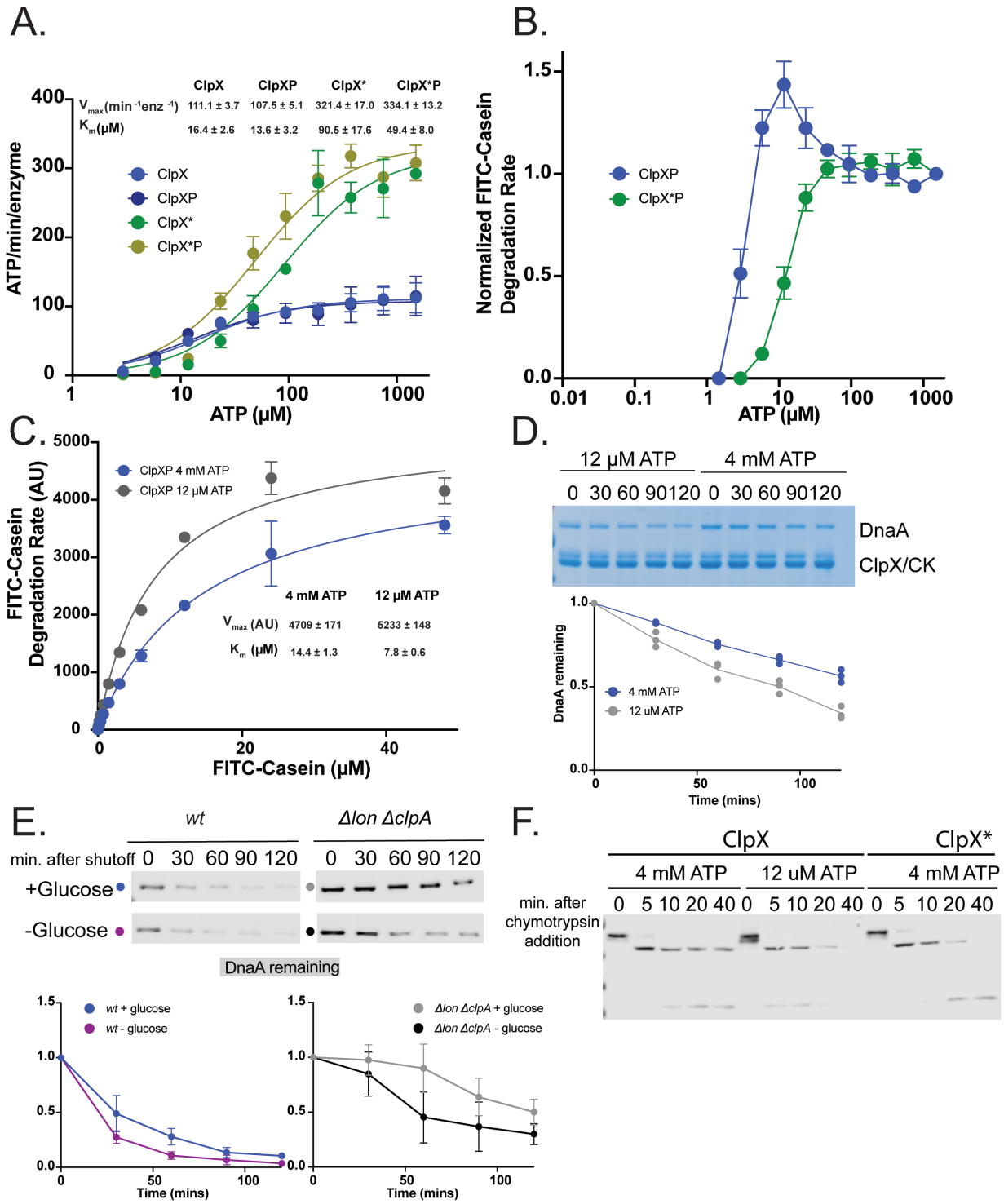

Figure 5: Limiting ATP alters wildtype ClpXP substrate specificity

A. Michaelis-Menten plot showing the rate of ClpX/ClpX* catalyzed ATP hydrolysis as a function of ATP concentration. Inset displays kinetic parameters. Assays were

performed with 0.1 μM ClpX or ClpX* hexamer, in the presence and absence of 0.2 μM ClpP. Data was fitted to Michaelis-Menten equation. Quantification of duplicate experiments.

B. FITC-Casein degradation by ClpXP or ClpX*P as a function of ATP concentration. Assays were performed with 0.1 μM ClpX or ClpX* hexamer, 0.2 μM ClpP, ATP regeneration system, and 50 μg/mL FITC-Casein. Quantification of duplicate experiments.

C. Michaelis-Menten plot showing the rate of degradation as a function of FITC-Casein concentration by ClpXP and ClpX*P under low and saturating ATP conditions. Inset displays kinetic parameters. Assays were performed with 0.1 μM ClpX or ClpX* hexamer, 0.2 μM ClpP, ATP regeneration system. Data was fitted to Michaelis-Menten equation. Quantification of triplicate experiments

D. *In vitro* degradation of DnaA by ClpXP under low and saturating ATP conditions. Assays were performed with 0.1 μM $ClpX_6$ or $ClpX_6$*, and 0.2 μM $ClpP_{14}$ and 0.5 μM DnaA. Quantification of triplicate experiments.

E. Antibiotic shutoff assays to monitor DnaA under ATP limiting conditions in *wt* and *Δlon ΔclpA* strains. Chloramphenicol was added to stop synthesis and lysates from samples at the indicated time points were used for western blot analysis. Quantifications of triplicate experiments shown to the right. Error bars represent SD.

F. Limited proteolysis assay to probe conformational states. ClpX was incubated with Chymotrypsin in Hepes buffer (20 mM Hepes pH 7.5, 100 mM KCl, 10 mM MgCl2, 10% glycerol) at 12 μM ATP and 4 mM ATP in the presence of ClpP and ATP regeneration system at 25 °C for the indicated time points. ClpX* was incubated with Chymotrypsin in Hepes buffer (20 mM Hepes pH 7.5, 100 mM KCl, 10 mM MgCl2, 10% glycerol) at 4 mM ATP in the presence of ClpP and ATP regeneration system at 25 °C for the indicated time points. ClpX was detected using anti-ClpX antibodies.

See also Figure S6.

Discussion

Because proteolysis is irreversible, degradation of substrates must be carefully monitored to avoid toxic consequences. In bacteria, different energy dependent proteases have distinct substrate preferences that allows them to collectively regulate proteome dynamics. However, how these energy-dependent proteases choose their target substrates from a pool of cellular proteins remains poorly understood. Certain determinants that dictate specificity include degrons, or degradation tags, such as the ssrA tag which marks proteins for degradation by ClpXP or ClpAP (Keiler, 2015; Keiler et al., 1996). Specificity can be augmented through adaptor proteins that help deliver substrates to proteases. For example, degradation of CtrA in *Caulobacter* is restricted to the ClpXP protease via a highly regulated series of adaptors (Joshi et al., 2015).

472

473 In this work, we identified a mutant allele of *clpX* (*clpX**) that compensates for the loss
474 of Lon through expanding ClpXP substrate specificity. The variant ClpX*P protease
475 complements the growth, motility, replication status, and morphology defects of a Δ*lon*
476 strain (Figure 1A-1C) by restoring levels and degradation of the Lon substrates DnaA
477 and SciP (Figure 2), which we confirm with biochemical experiments (Figure 3).
478 Interestingly, ClpX*P has an improved ability to degrade unfolded protein substrates, a
479 feature that likely explains the increased proteotoxic tolerance of Δ*lon clpX** strains
480 (Figure 3). Finally, this *clpX* variant is deficient in proteolysis of normal ClpXP
481 substrates, such as CtrA and ssrA-tagged proteins, suggesting a shift in substrate
482 preference rather than just an expansion (Figure 4). Mechanistic enzymology revealed
483 that ClpX* requires ~5-fold more ATP for saturation (Figure 5A), leading us to explore
484 the role of ATP levels in controlling specificity. Surprisingly, our *in vitro* studies found
485 that wildtype ClpXP is better at degrading unfolded proteins, DnaA, and SciP in ATP
486 limiting conditions, but worse at degrading ssrA-tagged proteins, similar to that seen
487 with ClpX*P in saturating ATP (Figure 5B, 5D, S6B). We recapitulate this effect *in vivo*,
488 showing that in starvation conditions that deplete ATP, DnaA degradation by wildtype
489 ClpXP is accelerated (Figure 5E). Our interpretation is that the ClpX oligomer adopts
490 distinct conformations in the ATP-saturated and ATP-limited conditions, as suggested
491 by limited proteolysis (Figure 5F).
492

493 How does altered ATP loading alter substrate recognition? Our working model is that
494 ClpX samples a 'open' state and a 'closed' state (Figure 6). Substrates can be captured
495 during the open-closed transition (as we propose for casein) or directly by the closed
496 state (as proposed for the ssrA tag and ClpX (Hersch *et al.*, 2005; Fei *et al.*, 2020).
497 Once a closed state engages a substrate, the unfoldase can processively translocate
498 the substrate to ClpP in the case of ClpXP (Figure 6). Recent cryo-EM structures reveal
499 shared features of substrate-bound AAA+ complexes, namely a shallow right-handed
500 ring with pore loops gripping the substrate and at least 4 ATP-bound protomers (Fei et
501 al., 2020; Gates et al., 2017; Lopez et al., 2020; Ripstein et al., 2020; Shin et al., 2020).
502 Consistent with our sampling model, substrate-free forms of these machines exhibit

503 more open, often left-handed, spiral structures (Shin et al., 2020; Yokom et al., 2016).
504 Interestingly, the original crystallization of ClpX shows a left-handed open spiral crystal
505 packing (Kim and Kim, 2003), similar to these substrate-free cryo-EM structures
506 described for other AAA+ machines. We propose that mutations or limiting ATP can
507 shift the open/closed balance to the more open state, which allows ClpX to better
508 capture certain substrates, such as unfolded proteins, which may not have as strict
509 sequence requirements for recognition. However, degrons such as the ssrA tag which
510 bind selectively to the closed conformation (Fei et al., 2020; Hersch et al., 2005) would
511 be poorly recognized in these conditions.
512
513 Prior work has shown that limiting nucleotide leads to loss of substrate degradation by
514 ClpXP (Martin et al., 2008), as would make sense for an ATP-fueled unfoldase.
515 However, we note that these studies exclusively used ssrA-tagged substrates, which
516 requires an ATP-bound (and presumably closed) form of ClpX for recognition. Thus,
517 the equivalent effects we are seeing here for casein, DnaA, and SciP would not have
518 been previously observed and also highlights the importance of using a range of
519 substrates in understanding activity. The open-capture / closed-processive model
520 described here also has precedence in the conformational states and activity of Hsp104
521 (Gates et al., 2017; Lee et al., 2019; Ye et al., 2020; Yokom et al., 2016), where doping
522 in nonhydrolyzable ATP analogs results in enhanced unfolding activity (Doyle et al.,
523 2007). In our current work, we have directly shown how different states of ClpX, favored
524 by either limiting ATP or mutation, can result in meaningful biological consequences, for
525 example by compensating for the loss of the Lon protease. Overall, we favor the
526 interpretation that exclusive substrate profiles for each AAA+ system are not hard-wired
527 but can be altered not only by mutations but also through modulation of ATP hydrolysis,
528 demonstrating a plasticity in these machines that yield flexibility in maintaining cellular
529 proteostasis.

Figure 6

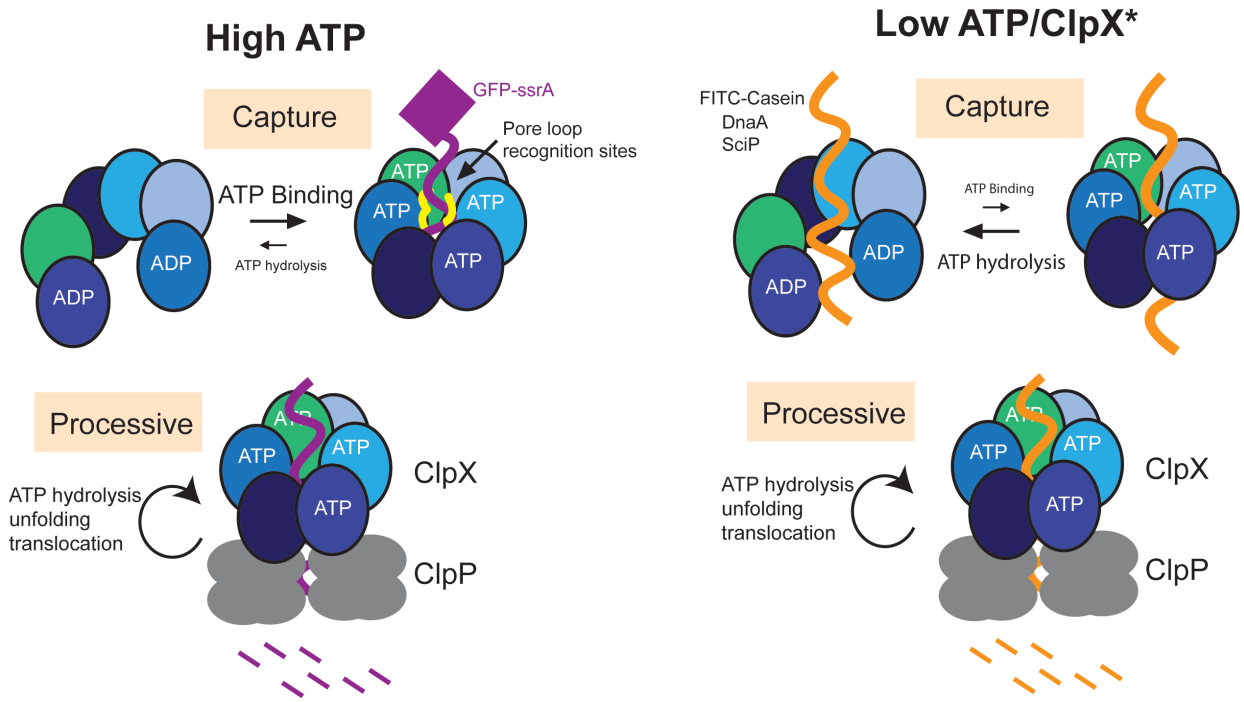

Figure 6: Model of ATP-dependent changes in ClpXP substrate specificity
ClpX exists in an equilibrium between an open and closed conformation. Under high ATP conditions, the closed conformation is favored, allowing ClpX to recognize and processively degrade certain substrates, such as GFP-ssrA, which makes sequence-specific contacts with pore loops of ClpX in a specific conformation (show in yellow). GFP-ssrA can then be unfolded and translocated to ClpP for irreversible degradation. Under low ATP conditions or in the presence of ClpX*, the balance shifts towards the open state, allowing ClpX to capture non-traditional classes of substrates, such as casein. ClpX can then switch to the closed state allowing processive degradation, unfolding, and translocation of captured substrate.

Materials and Methods

<u>Bacterial strains and growth conditions</u>

Bacterial strains and plasmids used in this study are listed in supplementary file 2. *Caulobacter crescentus* strains were grown in PYE medium (2g/L peptone, 1g/L yeast extract, 1 mM $MgSO_4$, and 0.5 mM $CaCl_2$) at 30°C. To generate strains, antibiotics were added to plates at the following concentrations: kanamycin (25 µg/ml), spectinomycin (100 µg/ml), and oxytetracycline (2 µg/ml). After initial selection steps for strain construction (excluding plasmids), antibiotics were excluded for all assays. For *C.*

550 *crescentus* motility assays, PYE with 0.3% agar was used and a single colony was
551 stabbed into the agar using a sterile tip and left to incubate at 30°C for 2 to 3 days.
552
553 *Escherichia coli* strains were grown in LB (10g/L NaCl, 10g/L tryptone, 5g/L yeast
554 extract) and supplemented with antibiotics at the following concentrations: ampicillin
555 (100 ug/ml), oxytetracycline (15 µg/ml), spectinomycin (50 µg/ml), kanamycin (50
556 µg/ml), gentamycin (20 µg/ml). For solid medium, 1.5% agar was used regardless of
557 bacterial species. For all strains, optical density was measured at 600 nm.
558
559 For induction purposes, the 477 plasmids were induced with xylose (0.2%) and
560 repressed with glucose (0.2%). For protein expression, 0.4 M IPTG was used for
561 induction.
562
563 **Cloning and strain constructions**
564 All *Caulobacter* strains were derived from CPC176, an isolate of NA1000. To generate
565 the *Δlon clpX** strain, a two-step recombination protocol with a sucrose counter
566 selection was utilized (Skerker et al., 2005). The vector pNPTS138 was digested with
567 HindIII and EcoRI. A PCR product of the *clpX** sequence was amplified from the original
568 motility suppressor and Gibson assembly was then used to generate pNPTS138_clpX*.
569 Following transformation with pNPTS138_clpX* into NA1000 or *Δlon*, primary selection
570 was on PYE supplemented with kanamycin. Primary colonies were grown overnight
571 without selection and overnight cultures were played on PYE agar supplemented with
572 3% w/v sucrose. To validate allelic swap, strains were tested for sensitivity to
573 kanamycin. *Δlon clpX** was also screened by motility and sequencing of the *clpX* locus
574 validated candidate clones.
575
576 *ClpX* or *clpX** merodiploid strains were generated by Gibson assembly of PCR product
577 and double digested plasmids of pMCS-2. The plasmids were then electroporated into
578 *Δlon* and selected onto kanamycin plates. Strains were validated by anti-ClpX westerns.
579

580 eGFP-ssrA(DAS) induction strains were generated by electroporating eGFP-ssrA(DAS)
581 477 plasmid into wildtype and wildtype *clpX** and selecting on spectinomycin. Strains
582 were validated by anti-M2 westerns.
583
584 **Motility Suppressor screen**
585 Transposon libraries were generated for *Δlon*. Two-liter PYE cultures were grown to mid
586 exponential phase, pelleted, and washed with 10% glycerol. Competent cells were
587 electroporated with Ez-Tn5 <Kan-2> transposome (Lucigen, Madison, WI). Cells
588 recovered for 90 minutes at 30 °C and then played on PYE plates supplemented with
589 kanamycin. Libraries were grown for 7 days. Colonies were then scraped from the
590 surface, combined, and resuspended to form a homogenous solution of PYE + 20%
591 glycerol.
592
593 The Tn library was thawed out and diluted into a flask containing two-liter 0.3% agar.
594 The cell agar mixture was plated and grown at 30 °C for 3 to 5 days. Candidates that
595 appeared motile were validated by innoculating single colonies into motility agar on the
596 same plate as NA1000 as a positive control and Δ*lon* as a negative control and
597 incubating plates for 2-3 days at 30 °C.
598
599 **Whole genome sequencing**
600 Genomic DNA was extracted using the MasterPure Complete DNA and RNA
601 purification kit (Epicenter Biotechnologies, Madison, WI). A Qubit Fluorometer
602 (ThermoFisher Scientific, Waltham, MA) was utilized to assess DNA concentration.
603 Illumina libraries were generated from the extracted genomic DNA using the NexteraXT
604 (Illumina, San Diego, CA) protocol. Libraries were multiplexed and sequenced at the
605 University of Massachusetts Amherst Genomics Core Facility on the NextSeq 500
606 (Illumina). Single nucleotide polymorphisms (SNPs) were detected using breseq
607 (Deatherage and Barrick, 2014).
608
609
610

611 **RNA sequencing**

612 RNA was extracted from stationary phase cells. Libraries were generated from the
613 extracted RNA using the NEB Next RNA Library Prep kits (NEB, Ipswich, MA). Libraries
614 were sequenced at the University of Massachusetts Genomics Core Facility on the
615 NextSeq 500 with single end 75 base reads. Reads were mapped to the *Caulobacter*
616 genome using BWA (Li and Durbin, 2009) and sorted with Samtools (Li et al., 2009).To
617 obtain the number of reads per gene, *bedtools map* (Quinlan and Hall, 2010) was used.
618 Rstudio and EdgeR was used to identify differentially expressed genes (R Core Team,
619 2019; Robinson et al., 2009).
620
621 Raw counts were normalized using the counts-per-million (CPM) method, and the
622 *edgeR* package in R was used to perform differential gene expression analysis, KEGG
623 pathway analysis, and FRY (Wu et al., 2010) gene set analysis. We filtered out any
624 gene that had less than 30 normalized counts across 3 or more samples. To test for
625 gene expression differences and identify differentially expressed genes across
626 experimental groups, we used the quasi-likelihood F-test. The over-representation
627 analysis for KEGG pathways done using the *kegga* function. FRY gene set analysis
628 done using the *fry* function. The CcrM, DnaA, and SciP regulons were obtained from
629 (Gonzalez et al., 2014; Hottes et al., 2005; Tan et al., 2010).
630

631 **Plating viability and drug sensitivity**

632 All Caulobacter strains were grown overnight in liquid PYE media. After overnight
633 growth, cells were back diluted to OD600 0.1 and outgrown to mid-exponential phase
634 before being normalized to OD_{600} 0.1 and 10-fold serially diluted on to media. For
635 experiments using mitomycin C (Sigma, St. Louis, MO) and L-canavanine (Sigma),
636 drugs were prepared at a stock concentration of 0.4 µg/ml mitomycin C, and 100 mg/ml
637 L-canavanine and filter sterilized. PYE agar was cooled before the drugs were added
638 and plates were left to air dry prior to serial dilution plating. All plates were incubated at
639 30℃ for 2-3 days and imaged with a gel doc.
640
641

642 ***In vivo* assays**

643 The stability of proteins *in vivo* was determined by inhibiting protein synthesis upon
644 addition of 30 µg/ml chloramphenicol to cells in exponential phase. At each time point,
645 1ml of culture was removed and centrifuged at 15,000 rpm for 2 minutes. The
646 supernatant was removed and pellets were flash frozen in liquid nitrogen. Pellets were
647 thawed, resuspended in 2x SDS dye, and normalized to the OD_{600} of the lowest sample.
648 Samples were boiled for 10 minutes and centrifuged for 10 minutes at 15,000 rpm.
649 Extracts were run on 10% Bis-Tris gels for 1 hour at room temperature at 150 V. Gels
650 were then transferred to nitrocellulose membranes for 1 hour at room temperature at
651 20V. Membranes were blocked with 3% milk in Tris-based saline with 0.05% Tween-20
652 (TBST) for 1 hour. Membranes were probed with primary antibody in 3% milk in TBST
653 at 4°C overnight with following dilution factors: 1:5000 dilution of DnaA, 1:5000 SciP,
654 1:5000 CcrM, 1:5000 ClpP, 1:2500 Lon, and 1:2000 M2. Membranes were washed with
655 1x TBST for 5 minutes three times and then probed with Licor secondary antibody with
656 1:10,000 dilution in 1x TBST at room temperature for 1 hour. The protein was visualized
657 using Licor Odyssey CLx. Bands were quantified using imageJ and degradation rates
658 were plotted using Prism.
659

660 To synchronize *Caulobacter* strains, cells were grown to an OD600 of 0.3-0.5 in PYE
661 and swarmer cells were isolated using Percoll density centrifugation. Cells were
662 released into PYE.

663 Flow cytometry was used to measure DNA content in rifampicin-treated cells as
664 previously described (Chen et al., 2009). Cells were rifampicin treated for three hours
665 prior to fixing in 70% ethanol.

666 **Carbon Starvation**

667 Cells were grown in M2G media (6.1 mM Na_2HPO_4, 3.9 mM KH_2PO_4, 9.3 mM NH_4Cl,
668 0.5 mM $MgSO_4$, 0.5 mM CaCl2, 10 µM $FeSO_4$ (EDTA chelate), 0.2% glucose). Cells
669 were then washed twice in cold M2G media (+glucose samples) or in M2 media (-
670 glucose samples) and resuspended in pre-warmed M2G or M2 media.

671 For bulk measurements of intracellular ATP, the Bactiter-Glo microbial cell viability
672 assay kit (Promega) was used. Cells were mixed with an equal volume of BacTiter-Glo
673 reagent in 384-well microtiter plates and incubated for five minutes before luminescence
674 was measured.

675 **Growth competition assay**

676 Overnight cultures of CPC798 were mixed with either *NA1000* or *clpX** at a 1:1 ratio.
677 Mixed strains were diluted into fresh PYE and allowed to outgrow for 12 doublings
678 overnight. The initial populations were verified by phase contrast and fluorescent
679 microscopy. Final ratios were normalized to their starting ratios. Data was plotted using
680 GraphPad Prism.

681 **Microscopy**

682 Phase contrast images of logarithmically growing cells were taken by Zeiss AXIO Scope
683 A1. Cells were mounted on 1% PYE agar pads and imaged using a 100X objective.
684 MicrobeJ (Ducret et al., 2016) for ImageJ (Schneider et al., 2012) was utilized to
685 quantify cell lengths. Stalk lengths were quantified using ImageJ. Prism was utilized for
686 representations of cell and stalk length measurements. Representative images of the
687 same scale were cropped to display morphological defects.

688 **Protein Purification and Modification**

689 Untagged Lon, untagged ClpX and ClpX*, and his-tagged ClpP were purified as
690 previously described (Chien et al., 2007; Goldberg et al., 1994; Gur and Sauer, 2008;
691 Levchenko et al., 2000). Titin-I27-β20 and Titin-I27-ssrA were purified as previously
692 described (Gur and Sauer, 2008; Kenniston et al., 2003) and labeled with Fluorescein-
693 5-maleimide (Thermo Scientific™) under guanidine hydrochloride denaturation. The
694 modified protein was buffer exchanged into H-buffer (20 mM Hepes pH 7.5, 100 mM
695 KCl, 10 mM MgCl2, 10% glycerol) and stored at 4°C. His_6SciP and his_6CtrA were
696 purified as described in (Gora et al., 2013). DnaA and CcrM were purified as his_6SUMO
697 tagged proteins, followed by tag cleavage as described (Jonas et al., 2013; Liu et al.,
698 2016; Wang et al., 2007). GFP-ssrA was purified as previously described (Yakhnin et

699 al., 1998). CtrA-RD+15 was purified as described (Smith et al., 2014). Detailed
700 purification protocols are available upon request.
701
702 ***In vitro* assays**
703 Degradation assays were performed at 30°C and monitored using SDS-PAGE gels as
704 described previously (Bhat et al., 2013). The final concentrations used can be found in
705 the figure legends. Densitometry was performed with ImageJ and degradation rates
706 were plotted using Prism.
707
708 Degradation of FITC-Casein, FT-Titin- β20, and FT-Titin-ssrA was monitored as an
709 increase in fluorescence over time. GFP-CtrARD+15 degradation was observed as a
710 loss of fluorescence over time as described previously (Smith et al., 2014).
711
712 ATP hydrolysis for ClpXP and ClpX*P was measured using a coupled kinase assay as
713 previously described (Burton et al., 2003)
714
715 **Limited Proteolysis**
716 To perform limited chymotrypsin digestion, 0.004 mg/mL chymotyrpsin was added to
717 0.01 mg/mL ClpX or ClpX* in the presence of ClpP and ATP regeneration system and
718 incubated at 25°C for indicated time points. To quench the reactions, 5X SDS dye
719 supplemented with 5 mM Protease inhibitor phenylmethylsulfonyl fluoride (PMSF) was
720 added to quench the reactions. The samples were run on a 10% Bis-Tris gel and
721 transferred to nitrocellulose as described above. Membranes were probed with primary
722 antibody in 3% milk in TBST at 4°C overnight with following dilution factors: 1:5000
723 dilution of ClpX. Membranes were washed with 1x TBST for 5 minutes three times and
724 then probed with Licor secondary antibody with 1:10,000 dilution in 1x TBST at room
725 temperature for 1 hour. The protein was visualized using Licor Odyssey CLx.
726
727
728
729

Acknowledgements

We thank the Chien, Strieter, Stratton, and Serio lab members for helpful comments and discussion on the manuscript. S.A.M. and B.A. were supported in part through the UMass NIH Chemistry Biology Interface Training Program (NIH T32GM008515) and S.A.M. in part by the HHMI Gilliam Fellowship program. Work in the Chien lab is funded by the NIH (R35GM130320). We thank the Genomics Resource Laboratory (Institute for Applied Life Sciences; University of Massachusetts Amherst) and the Mass Spectrometry Core Facilities for services and equipment support.

Author Contributions: Conceptualization: S.A.M. and P.C.; Investigation, S.A.M. and B.A.; Writing, S.A.M and P.C.; Funding Acquisition, P.C. Supervision, P.C.

Declaration of Interests: The authors declare no competing interests

References

Baker, T.A., and Sauer, R.T. (2012). ClpXP, an ATP-powered unfolding and protein-degradation machine. Biochim. Biophys. Acta - Mol. Cell Res. *1823*, 15–28.

Bhat, N.H., Vass, R.H., Stoddard, P.R., Shin, D.K., and Chien, P. (2013). Identification of ClpP substrates in Caulobacter crescentus reveals a role for regulated proteolysis in bacterial development. *88*, 1083–1092.

Breidenstein, E.B.M., Janot, L., Strehmel, J., Fernandez, L., Taylor, P.K., Kukavica-Ibrulj, I., Gellatly, S.L., Levesque, R.C., Overhage, J., and Hancock, R.E.W. (2012). The Lon Protease Is Essential for Full Virulence in Pseudomonas aeruginosa. PLoS One *7*.

Chen, Y.E., Tsokos, C.G., Biondi, E.G., Perchuk, B.S., and Laub, M.T. (2009). Dynamics of two phosphorelays controlling cell cycle progression in Caulobacter crescentus. J. Bacteriol. *191*, 7417–7429.

Chien, P., Perchuk, B.S., Laub, M.T., Sauer, R.T., and Baker, T. a (2007). Direct and adaptor-mediated substrate recognition by an essential AAA+ protease. Proc. Natl. Acad. Sci. U. S. A. *104*, 6590–6595.

Chowdhury, T., Chien, P., Ebrahim, S., Sauer, R.T., and Baker, T.A. (2010). Versatile modes of peptide recognition by the ClpX N domain mediate alternative adaptor-binding specificities in different bacterial species. Protein Sci. *19*, 242–254.

Deatherage, D.E., and Barrick, J.E. (2014). Identification of mutations in laboratory

evolved microbes from next-generation sequencing data using breseq. Methods Mol Biol. 165–188.

Domian, I.J., Reisenauer, a, and Shapiro, L. (1999). Feedback control of a master bacterial cell-cycle regulator. Proc. Natl. Acad. Sci. U. S. A. *96*, 6648–6653.

Doyle, S.M., Shorter, J., Zolkiewski, M., Hoskins, J.R., Lindquist, S., and Wickner, S. (2007). Asymmetric deceleration of ClpB or Hsp104 ATPase activity unleashes protein-remodeling activity. Nat. Struct. Mol. Biol. *14*, 114–122.

Ducret, A., Quardokus, E.M., and Brun, Y. V. (2016). MicrobeJ, a tool for high throughput bacterial cell detection and quantitative analysis. Nat. Microbiol. *1*, 1–7.

Farrell, C.M., Baker, T.A., and Sauer, R.T. (2007). Altered Specificity of a AAA+ Protease. Mol. Cell *25*, 161–166.

Fei, X., Bell, T.A., Barkow, S.R., Baker, T.A., and Sauer, R.T. (2020). Structural basis of clpxp recognition and unfolding of ssra-tagged substrates. Elife *9*, 1–39.

Gates, S.N., Yokom, A.L., Lin, J., Jackrel, M.E., Rizo, A.N., Kendsersky, N.M., Buell, C.E., Sweeny, E.A., Mack, K.L., Chuang, E., et al. (2017). Ratchet-like polypeptide translocation mechanism of the AAA+ disaggregase Hsp104. Science (80-.). *357*, 273–279.

Goff, S.A., Casson, L.P., and Goldberg, A.L. (1984). Heat shock regulatory gene htpR influences rates of protein degradation and expression of the lon gene in Escherichia coli. Proc. Natl. Acad. Sci. U. S. A. *81*, 6647–6651.

Goldberg, A.L. (1972). Degradation of Abnormal Proteins in Escherichia coli. Proc Natl Acad Sci U S A *69*, 422–426.

Goldberg, A.L., Moerschell, R.P., Hachung, C., and Maurizi, M.R. (1994). ATP-dependent protease La (Lon) from Escherichia coli. Methods Enzymol. *244*, 350–375.

Gonzalez, D., Kozdon, J.B., McAdams, H.H., Shapiro, L., and Collier, J. (2014). The functions of DNA methylation by CcrM in Caulobacter crescentus: A global approach. Nucleic Acids Res. *42*, 3720–3735.

Gora, K.G., Cantin, A., Wohlever, M., Joshi, K.K., Perchuk, B.S., Chien, P., and Laub, M.T. (2013). Regulated proteolysis of a transcription factor complex is critical to cell cycle progression in Caulobacter crescentus. Mol. Microbiol. *87*, 1277–1289.

Gorbatyuk, B., and Marczynski, G.T. (2005). Regulated degradation of chromosome replication proteins DnaA and CtrA in Caulobacter crescentus. Mol. Microbiol. *55*, 1233–1245.

815 Gottesman, S., Roche, E., Zhou, Y.N., and Sauer, R.T. (1998). The ClpXP and ClpAP
816 proteases degrade proteins with carboxy-terminal peptide tails added by the SsrA-
817 tagging system. Genes Dev. *12*, 1338–1347.
818 Gur, E., and Sauer, R.T. (2008). Recognition of misfolded proteins by Lon, a AAA+
819 protease. Genes Dev. *22*, 2267–2277.
820
821 Gur, E., Biran, D., and Ron, E.Z. (2011). Regulated proteolysis in Gram-negative
822 bacteria — how and when? Nat Rev Microbiol *9*, 839–848.
823
824 Hersch, G.L., Burton, R.E., Bolon, D.N., Baker, T.A., and Sauer, R.T. (2005).
825 Asymmetric interactions of ATP with the AAA+ ClpX6 unfoldase: Allosteric control of a
826 protein machine. Cell *121*, 1017–1027.
827
828 Hottes, A.K., Shapiro, L., and McAdams, H.H. (2005). DnaA coordinates replication
829 initiation and cell cycle transcription in Caulobacter crescentus. Mol. Microbiol. *58*,
830 1340–1353.
831
832 Howard-Flanders, P., Simson, E., and Theriot, L. (1964). A locus that controls filament
833 formation and sensitiviry to radiation in Escherichia coli K-12. Genetics *49*, 237–246.
834
835 Hulsen, T., de Vlieg, J., and Alkema, W. (2008). BioVenn - A web application for the
836 comparison and visualization of biological lists using area-proportional Venn diagrams.
837 BMC Genomics *9*, 1–6.
838
839 Jenal, U., and Fuchs, T. (1998). An essential protease involved in bacterial cell-cycle
840 control. EMBO J. *17*, 5658–5669.
841
842 Jonas, K., Liu, J., Chien, P., and Laub, M.T. (2013). Proteotoxic stress induces a cell-
843 cycle arrest by stimulating lon to degrade the replication initiator DnaA. Cell *154*, 623–
844 636.
845
846 Joshi, K.K., Bergé, M., Radhakrishnan, S.K., Viollier, P.H., and Chien, P. (2015). An
847 Adaptor Hierarchy Regulates Proteolysis during a Bacterial Cell Cycle. Cell *163*, 419–
848 431.
849
850 Keiler, K.C. (2015). Mechanisms of ribosome rescue in bacteria. Nat. Rev. Microbiol.
851 *13*, 285–297.
852
853 Keiler, K.C., Waller, P.R.H., and Sauer, R.T. (1996). Role of a Peptide Tagging System
854 in Degradation of Proteins Synthesized from Damaged Messenger RNA. Sci. *271*,
855 990–993.
856
857 Kenniston, J.A., Baker, T.A., Fernandez, J.M., and Sauer, R.T. (2003). Linkage between
858 ATP consumption and mechanical unfolding during the protein processing reactions of
859 an AAA+ degradation machine. Cell *114*, 511–520.
860

861 Kim, D.Y., and Kim, K.K. (2003). Crystal Structure of ClpX Molecular Chaperone from
862 Helicobacter pylori. J. Biol. Chem. *278*, 50664–50670.
863
864 Langklotz, S., Baumann, U., and Narberhaus, F. (2012). Structure and function of the
865 bacterial AAA protease FtsH. Biochim. Biophys. Acta - Mol. Cell Res. *1823*, 40–48.
866
867 Laub, M.T., Chen, S.L., Shapiro, L., and McAdams, H.H. (2002). Genes directly
868 controlled by CtrA, a master regulator of the Caulobacter cell cycle. Proc. Natl. Acad.
869 Sci. U. S. A. *99*, 4632–4637.
870
871 Lee, I., and Suzuki, C.K. (2008). Functional mechanics of the ATP-dependent Lon
872 protease- lessons from endogenous protein and synthetic peptide substrates. Biochim.
873 Biophys. Acta - Proteins Proteomics *1784*, 727–735.
874
875 Lee, S., Roh, S.H., Lee, J., Sung, N., Liu, J., and Tsai, F.T.F. (2019). Cryo-EM
876 Structures of the Hsp104 Protein Disaggregase Captured in the ATP Conformation. Cell
877 Rep. *26*, 29-36.e3.
878
879 Levchenko, I., Seidel, M., Sauer, R.T., and Baker, T.A. (2000). A Specificity-Enhancing
880 Factor for the ClpXP Degradation Machine. Science (80-.). *289*, 2354–2356.
881
882 Li, H., and Durbin, R. (2009). Fast and accurate short read alignment with Burrows-
883 Wheeler transform. Bioinformatics *25*, 1754–1760.
884
885 Li, H., Handsaker, B., Wysoker, A., Fennell, T., Ruan, J., Homer, N., Marth, G.,
886 Abecasis, G., and Durbin, R. (2009). The Sequence Alignment/Map format and
887 SAMtools. Bioinformatics *25*, 2078–2079.
888
889 Liu, J., Francis, L.I., Jonas, K., Laub, M.T., and Chien, P. (2016). ClpAP is an auxiliary
890 protease for DnaA degradation in Caulobacter crescentus. Mol. Microbiol. *102*, 1075–
891 1085.
892
893 Lopez, K.E., Rizo, A.N., Tse, E., Lin, J.B., Scull, N.W., Thwin, A.C., Lucius, A.L.,
894 Shorter, J., and Southworth, D.R. (2020). Conformational plasticity of the ClpAP AAA+
895 protease couples protein unfolding and proteolysis. Nat. Struct. Mol. Biol. *27*, 406–416.
896
897 Mahmoud, S.A., and Chien, P. (2018). Regulated Proteolysis in Bacteria. Annu. Rev.
898 Biochem. *87*, 677–696.
899
900 Martin, A., Baker, T.A., and Sauer, R.T. (2008). Protein unfolding by a AAA+ protease is
901 dependent on ATP-hydrolysis rates and substrate energy landscapes. Nat. Struct. Mol.
902 Biol. *15*, 139–145.
903
904 Mizusawa, S., and Gottesman, S. (1983). Protein degradation in Escherichia coli: the
905 lon gene controls the stability of sulA protein. Proc. Natl. Acad. Sci. U. S. A. *80*, 358–
906 362.

907
908 Persat, A., Stone, H.A., and Gitai, Z. (2014). The curved shape of caulobacter
909 crescentus enhances surface colonization in flow. Nat. Commun. *5*, 1–9.
910 Quinlan, A.R., and Hall, I.M. (2010). BEDTools: a flexible suite of utilities for comparing
911 genomic features. Bioinformatics *26*, 841–842.
912
913 Quon, K.C., Marczynski, G.T., and Shapiro, L. (1996). Cell cycle control by an essential
914 bacterial two-component signal transduction protein. Cell *84*, 83–93.
915
916 R Core Team (2019). R: A language and Environment for Statistical Computing (R
917 Foundation for Statistical Computing).
918
919 Ripstein, Z.A., Vahidi, S., Houry, W.A., Rubinstein, J.L., and Kay, L.E. (2020). A
920 processive rotary mechanism couples substrate unfolding and proteolysis in the ClpXP
921 degradation machinery. Elife *9*.
922
923 Robinson, M.D., McCarthy, D.J., and Smyth, G.K. (2009). edgeR: A Bioconductor
924 package for differential expression analysis of digital gene expression data.
925 Bioinformatics *26*, 139–140.
926
927 Rogers, A., Townsley, L., Gallego-hernandez, A.L., Beyhan, S., Kwuan, L., and Yildiz,
928 F.H. (2016). and the Type VI Secretion System in Vibrio cholerae. *198*, 973–985.
929
930 Sauer, R.T., and Baker, T.A. (2011). AAA+ Proteases: ATP-Fueled Machines of Protein
931 Destruction. Annu. Rev. Biochem *80*, 587–612.
932
933 Schneider, C.A., Rasband, W.S., and Eliceiri, K.W. (2012). NIH Image to ImageJ: 25
934 years of image analysis. Nat. Methods *9*, 671–675.
935
936 Shin, M., Puchades, C., Asmita, A., Puri, N., Adjei, E., Luke Wiseman, R., Wali Karzai,
937 A., and Lander, G.C. (2020). Structural basis for distinct operational modes and
938 protease activation in AAA+ protease Lon.
939
940 Skerker, J.M., Prasol, M.S., Perchuk, B.S., Biondi, E.G., and Laub, M.T. (2005). Two-
941 component signal transduction pathways regulating growth and cell cycle progression in
942 a bacterium: A system-level analysis. PLoS Biol. *3*.
943
944 Smith, S.C., Joshi, K.K., Zik, J.J., Trinh, K., Kamajaya, A., Chien, P., and Ryan, K.R.
945 (2014). Cell cycle-dependent adaptor complex for ClpXP-mediated proteolysis directly
946 integrates phosphorylation and second messenger signals. Proc. Natl. Acad. Sci. U. S.
947 A. *111*, 14229–14234.
948
949 Tan, H.M., Kozdon, J.B., Shen, X., Shapiro, L., and McAdams, H.H. (2010). An
950 essential transcription factor, SciP, enhances robustness of Caulobacter cell cycle
951 regulation. Proc. Natl. Acad. Sci. U. S. A. *107*, 18985–18990.
952

Wang, K.H., Sauer, R.T., and Baker, T.A. (2007). ClpS modulates but is not essential for bacterial N-end rule degradation. Genes Dev. *21*, 403–408.

Witkin, E.M. (1946). Inherited Differences in Sensitivity to Radiation in Escherichia Coli. Proc. Natl. Acad. Sci. U. S. A. *32*, 59–68.

Wortinger, M., Sackett, M.J., and Brun, Y. V. (2000). CtrA mediates a DNA replication checkpoint that prevents cell division in Caulobacter crescentus. EMBO J. *19*, 4503–4512.

Wright, R., Stephens, C., Zweiger, G., Shapiro, L., and Alley, M.R.K. (1996). Caulobacter Lon protease has a critical role in cell-cycle control of DNA methylation. Genes Dev. *10*, 1532–1542.

Wu, D., Lim, E., Vaillant, F., Asselin-Labat, M.L., Visvader, J.E., and Smyth, G.K. (2010). ROAST: Rotation gene set tests for complex microarray experiments. Bioinformatics *26*, 2176–2182.

Yakhnin, A. V., Vinokurov, L.M., Surin, A.K., and Alakhov, Y.B. (1998). Green fluorescent protein purification by organic extraction. Protein Expr. Purif. *14*, 382–386.

Ye, X., Lin, J., Mayne, L., Shorter, J., and Walter Englander, S. (2020). Structural and kinetic basis for the regulation and potentiation of Hsp104 function. Proceeding Natl. Acad. Sci. .

Yokom, A.L., Gates, S.N., Jackrel, M.E., Mack, K.L., Su, M., Shorter, J., and Southworth, D.R. (2016). Spiral architecture of the Hsp104 disaggregase reveals the basis for polypeptide translocation. Nat. Struct. Mol. Biol. *23*, 830–837.

Zeinert, R.D., Liu, J., Yang, Q., Du, Y., Haynes, C.M., and Chien, P. (2018). A legacy role for DNA binding of Lon protects against genotoxic stress. BioRxiv.

Supplemental Figure Legends

Figure S1: Validation of motility screen suppressor

(A-B) Motility assay on 0.3% PYE agar of indicated strains.

C. Sequence alignment of ClpX homologs. Conserved glycine residue and walker B motif are marked.

D. Quantification of the percent of cells with DNA content of 1N, 2N, and >2N in *wt*, *Δlon,* and *Δlon clpX** strains.

Figure S2: RNA-seq gene set analysis

(A-B) Volcano plot showing the transcriptional differences of Δ*lon* compared to *wt* (left) and *Δlon clpX** compared to *wt* (right), as measured by RNA-seq. The negative $\log_{10}$ of the p value is plotted against $\log_2$ of the fold change mRNA counts. Genes that are marked in red have an FDR <0.05. Transcripts that are associated with either the SciP regulon (Tan et al., 2010) or cell cycle (KEGG pathways) are highlighted in blue.

C. Kyoto Encyclopedia of Genes and Genomes (KEGG) pathway enrichment analysis and FRY gene set analysis. FRY gene set analysis performed using *fry* function from *edgeR* package in R (Robinson et al., 2009; Wu et al., 2010). The CcrM, DnaA, and SciP regulons were assigned according to (Gonzalez et al., 2014; Hottes et al., 2005; Tan et al., 2010). Over-represented pathways in KEGG pathway database identified using the *kegga* function from *edgeR* package in R.

Figure S3: *clpX mutant is dominant**

A. Western blot showing CcrM levels in synchronized populations of wt, *Δlon, and Δlon clpX** cells. Swarmer cells were isolated using a density gradient and an equal number of cells were released into fresh PYE medium. Samples were withdrawn at the indicated time points and probed with anti-CcrM.

B**.** Growth curves of *wild type* (wt), *Δlon, and Δlon* merodiploid with second copy of *clpX** at native locus*.* Cells grown in PYE.

C. Spot assays comparing colony formation of strains in PYE and PYE supplemented with mitomycin C.

D. Motility assay on 0.3% PYE agar of indicated strains

Figure S4: *In vitro* characterization of ClpX*

A. ATPase activity of 0.1 μM ClpX/ClpX* plus 0.2 μM ClpP is displayed. Triplicate experiments are shown.

B. *In vitro* degradation of CcrM by 0.2 μM Lon is shown as a control. The bottom gel shows CcrM degradation assay in the presence of ATP, with no regeneration mix.

C. FITC-Casein titration in the presence of either ClpXP or ClpX*P. Data was fit to the Michaelis-Menten equation. ClpX*P degrades FITC-Casein 2-3 fold better than ClpXP. Inset shows residual plot for Michaelis-Menten fit

F. Fluorescin-*Titin*-I27-β20 titration in the presence of either ClpXP or ClpX*P. Data was fit to the Michaelis-Menten equation. V_{max}/K_M was 30% higher for ClpX*P in comparison to ClpXP. Inset shows residual plot for Michaelis-Menten fit.

1045 **Figure S5 ClpX*P is deficient in native substrate degradation**
1046 A. *In vitro* degradation of GFP-ssrA.
1047 B. Fluorescein-*Titin*-I27-ssrA titration in the presence of either ClpXP or ClpX*P. Data
1048 was fit to the Michaelis-Menten equation. V_{max}/K_M was 30% lower for ClpX*P in
1049 comparison to ClpXP. Inset shows residual plot for Michaelis-Menten fit.
1050 C. *In vitro* fluorescence degradation assay of eGFP-CtrA-RD+15 in the presence of
1051 adaptors. Degradation assays were performed with 1 μM eGFP-CtrA-RD+15, 0.1 μM
1052 ClpX or ClpX* hexamer, 0.2 μM ClpP, 2 μM CpdR, 1 μM RcdA, 1 μM PopA, and 20 μM
1053 cyclic di-GMP, and ATP regeneration system.
1054
1055
1056 **Figure S6: Modulating ATP changes substrate preferences**
1057 A. GFP-ssrA degradation by ClpXP or ClpX*P as a function of ATP concentration.
1058 Assays were performed with 0.1 μM ClpX or ClpX* hexamer, 0.2 μM ClpP, ATP
1059 regeneration system, and 10 μM GFP-ssrA.
1060 B. *In vitro* degradation of SciP by ClpXP under low and saturating ATP conditions.
1061 Assays were performed with 0.1 μM $ClpX_6$ or $ClpX_6$*, and 0.2 μM $ClpP_{14}$ and 5 μM SciP.
1062 Quantification of triplicate experiments shown.
1063 C. Relative intracellular ATP concentrations measured using a luciferase-based assay
1064 during the course of antibiotic shutoff assay.
1065
1066
1067
1068
1069
1070
1071
1072
1073
1074

Figure S1 - related to figure 1

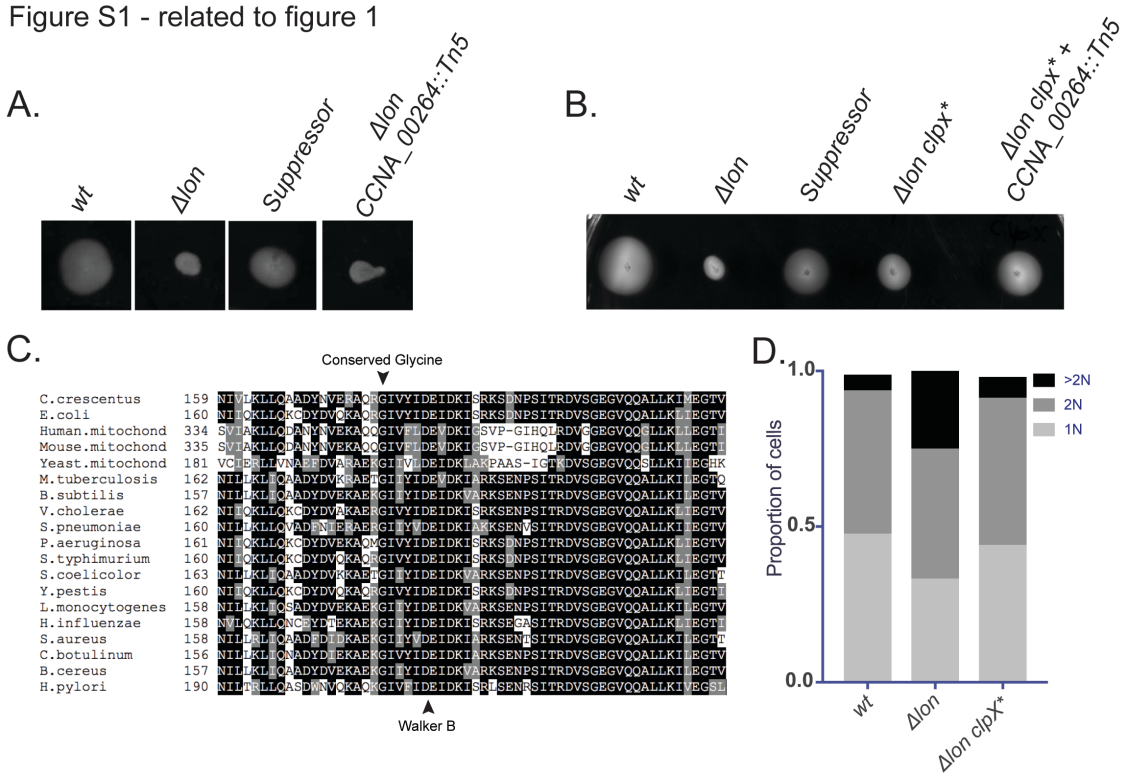

1075
1076

Figure S2- Related to Figure 2

A.

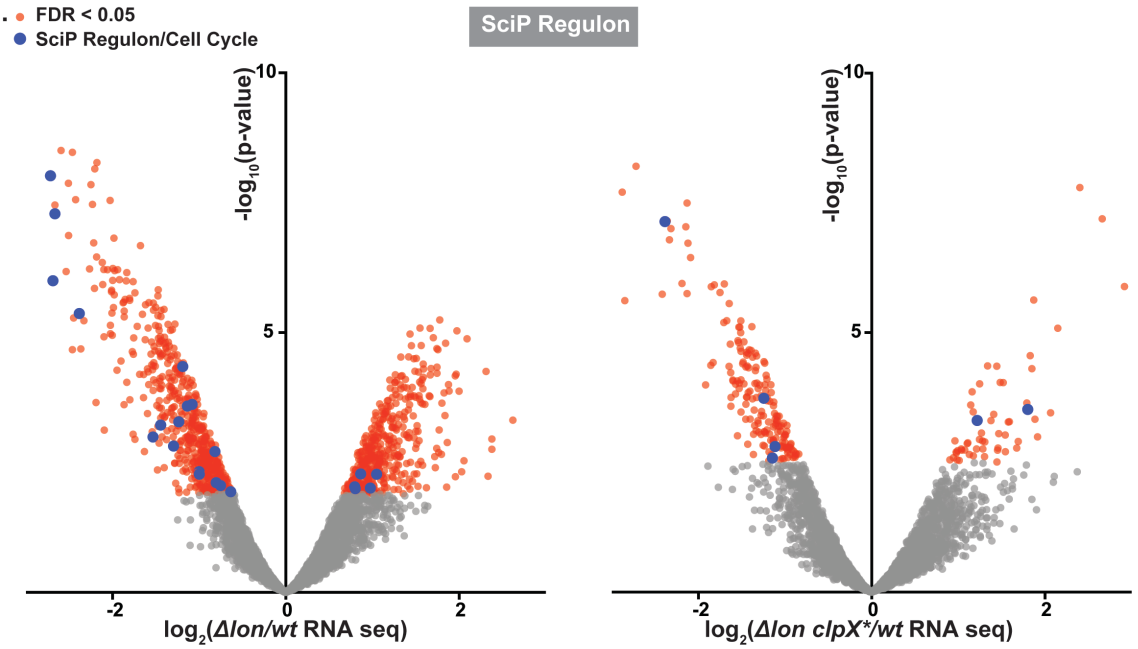

B.

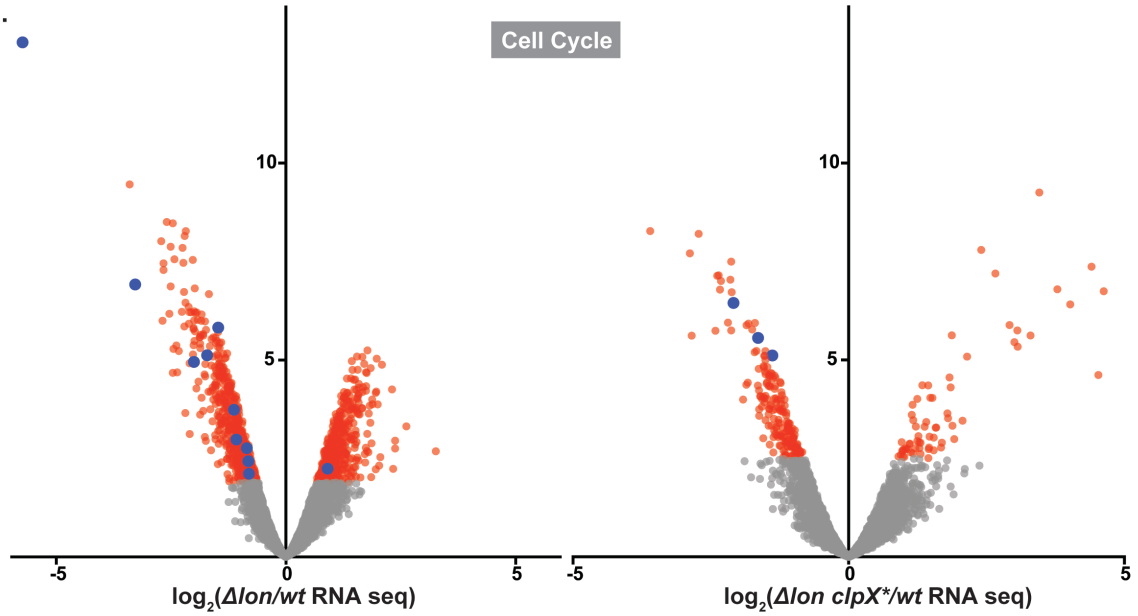

C.

FRY Gene Set Analysis

	Δlon vs *wt*				Δlon clpX* vs wt			
	Number of Genes	Direction	p-value	FDR	Number of Genes	Direction	p-value	FDR
SciP	61	Down	0.0029	0.0044	61	Down	0.3391	0.5042
CcrM	504	Up	0.0014	0.0014	504	Up	0.7391	0.7391
DnaA	32	Down	0.0989	0.0980	32	Down	0.0919	0.1275

KEGG Enrichment Analysis

	Cell Cycle		
	Number of Genes	Direction	p-value
Δlon vs wt	31	10, Down	0.0086
Δlon clpX vs wt*	31	3, Down	0.1725

1077

Figure S3- Related to Figure 2

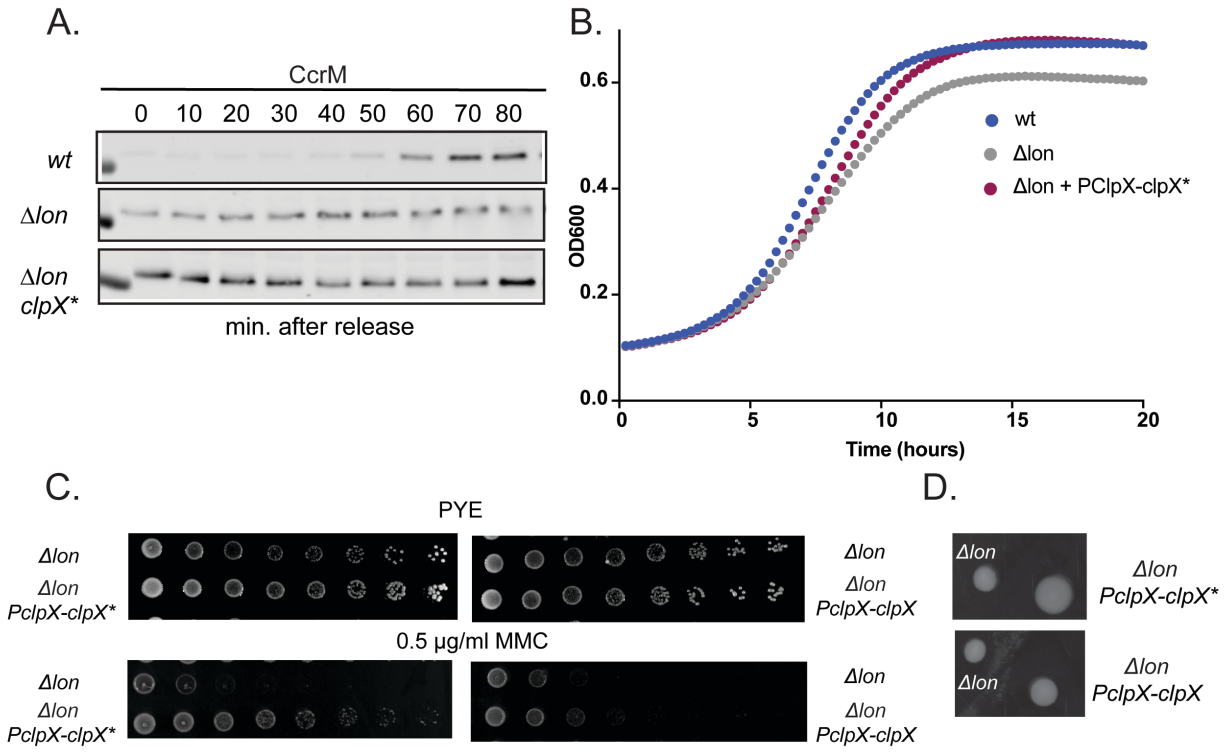

1078

Figure S4- Related to Figure 3

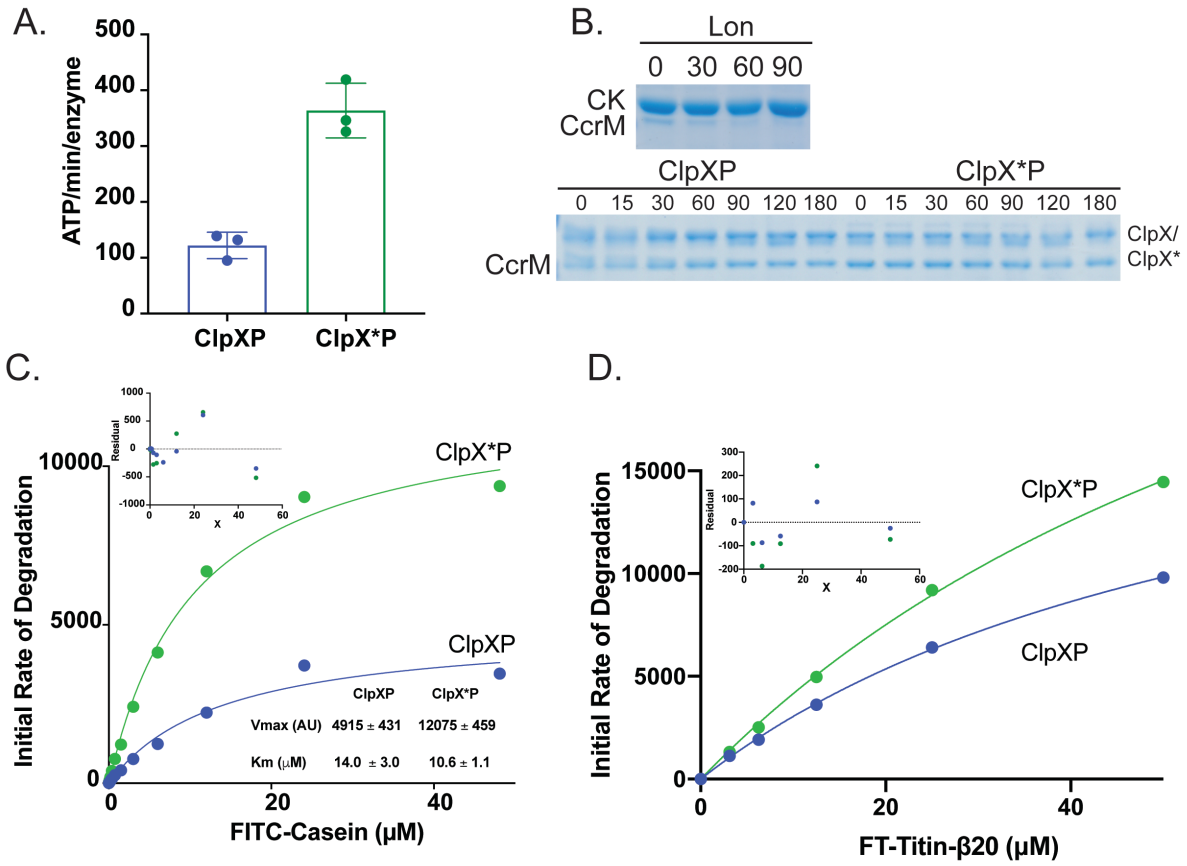

1079

Figure S5- Related to Figure 4

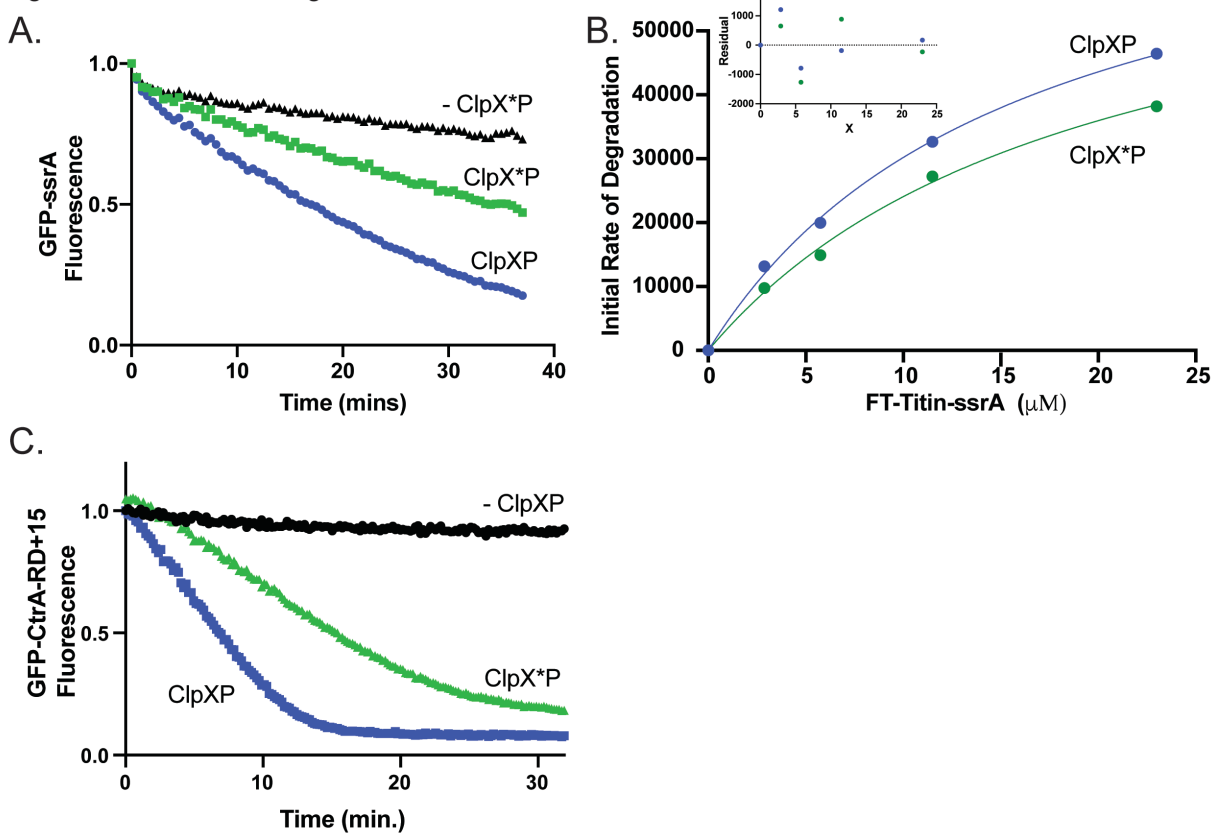

1080

Figure S6- Related to Figure 5

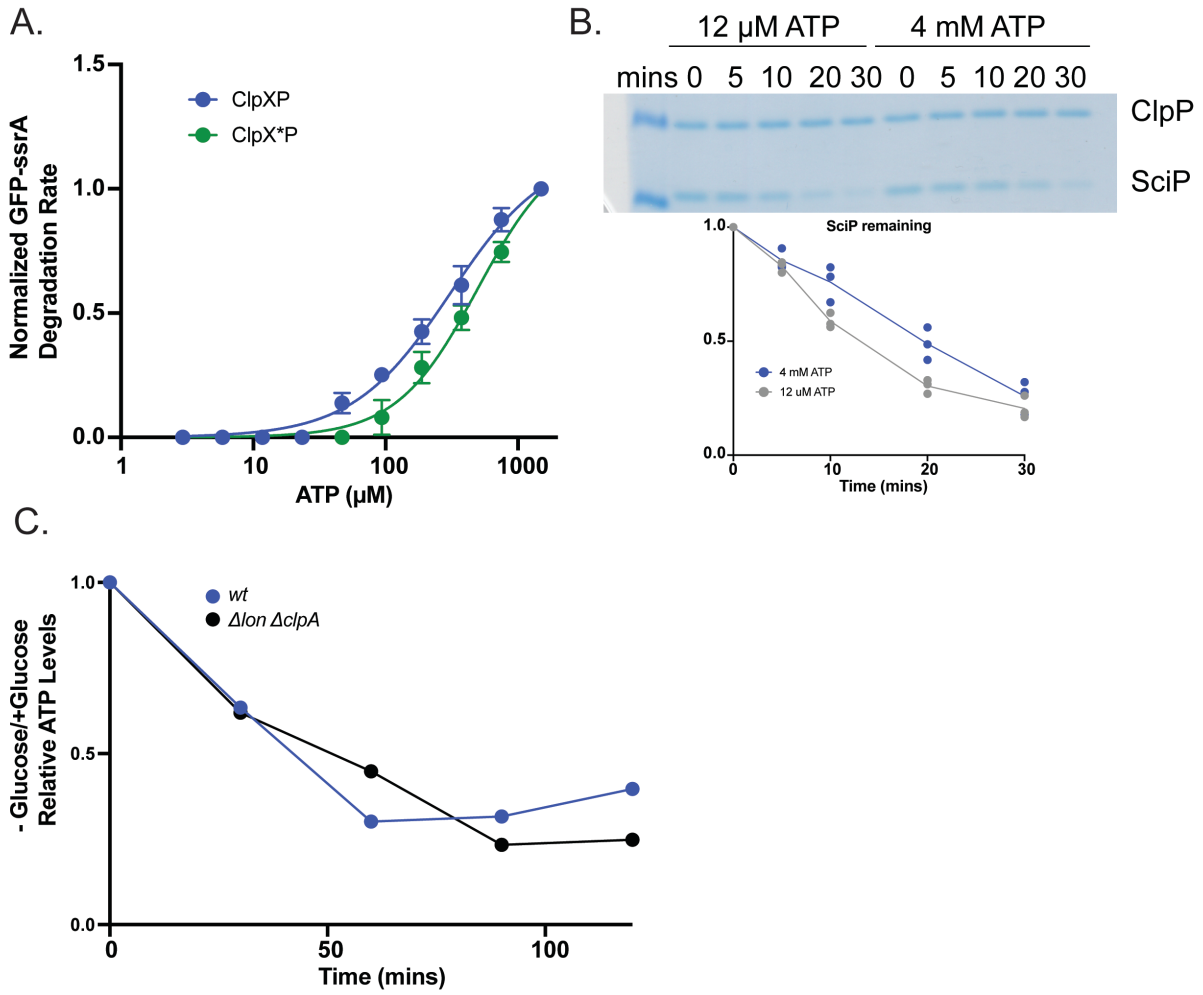

1081